

An “uncertainty region” reduced basis approach to parameter estimation for linear parabolic partial differential equations

N. C. Nguyen¹, M. A. Grepl¹, A. T. Patera¹ and G. R. Liu²

¹ Department of Mechanical Engineering, Massachusetts Institute of Technology, 77 Massachusetts Ave, Cambridge, MA 02139, USA

² Department of Mechanical Engineering, National University of Singapore, 10 Kent Ridge Crescent, Singapore 119260, Singapore

E-mail: cuongng@mit.edu

Abstract. We present an inverse problem procedure for the efficient calculation of approximations to the parametric “uncertainty region.” The uncertainty region is the compact set of all parameter values consistent with interval (experimental) output measurements; we provide a series of approximate uncertainty regions from less rigorous and very fast — for initial design — to fully rigorous and less fast — for final confirmation. The dependence of the uncertainty region on the magnitude of the experimental error distinguishes identifiable and non-identifiable inverse problems; for the former, our approach can further provide quantitative and sharp prediction of the unknown parameter value, the associated (experimentally and numerically induced) uncertainty, and the sensitivity to measurement protocol. The method depends critically on a Reduced Basis (RB) output bound evaluator for the forward problem: the RB output *prediction* provides the very fast response needed (to effect the many queries required) to construct the approximate uncertainty region; the RB output *bound* ensures that we control (optimize) and rigorously incorporate the numerical error in our inverse analysis. We develop the technique for (parametrically coercive) linear parabolic partial differential equations such as the transient heat conduction equation; as an example, we consider detection and characterization of de-lamination cracks in Fiber-Reinforced Polymer surface treatment of concrete structures.

Submitted to: *Inverse Problems*

1. Introduction

Engineering analyses often requires the prediction of partial differential equation (PDE) outputs — related to temperatures, flowrates, or heat fluxes — as functions of an input parameter vector — related to geometry, physical properties, boundary conditions, or loads. These outputs are typically expressed as functionals of field variables such as temperature, displacement, or velocity associated with the parametrized PDE which describes the underlying physics. The *forward* problem consists of evaluating the outputs for any given input parameter vector, which in turn necessitates solution of the underlying PDE. In contrast, the parameter estimation/*inverse* problem consists of estimating the input parameter vector from experimental measurements of the outputs, which typically necessitates many realizations of the forward problem.

There are a variety of approaches to inverse problems and uncertainty quantification more generally. The *regularization approach* [9, 29, 30, 31] is widely used to address *ill-posed* problems that arise due to insufficient and noisy data. We refer to [30, 31] for fundamentals of the Tikhonov regularization method and [2] (and references therein) for alternative regularization techniques. It should be noted that most regularization methods find only one solution corresponding to given specific data, and hence do not quantify the implications of uncertainty on the parameter prediction. *Bayesian statistical methods* [7, 10, 21, 36] and Monte Carlo simulation [20, 16] provide for robust and systematic analysis of inverse problems. However, the methods can not readily address problems of uncertainty analysis in which the probability distributions of the measurements are not known and can not easily be subjectively/plausibly proposed. Both regularization and Bayesian techniques are often applied to PDE parameter estimation problems.

For PDE parameter estimation problems, classical discretization methods such as the finite element, finite volume, and finite difference methods can be too expensive

for many applications, in particular *real-time* applications. In some cases in which the parameters do not appear in the operator, real-time approaches can be developed; for example, a real-time estimation technique for (ill-posed) inverse heat conduction problems is discussed in [1, 3]. However, in most cases, these techniques can not readily treat problems in which the differential operator is parameter-dependent, and hence for which (say) the relevant singular value decomposition can not be readily pre-computed. Our emphasis is precisely in extending real-time approaches to cases in which the parameters enter into the PDE operator.

Towards that end, Reduced Basis (RB) output bound methods [18, 23, 26] can effectively serve in many of the above-mentioned inverse problem approaches, providing for extremely accurate and rapid forward evaluation without — thanks to rigorous *a posteriori* error estimation — introducing a new source of uncontrolled (numerical) uncertainty. The essential components of RB methods are (a) rapidly convergent global RB approximations — (Galerkin) projection onto a space W_N spanned by solutions of the governing PDE at N judiciously selected points in parameter space; (b) *a posteriori* error estimation — procedures that provide rigorous and sharp bounds for the error in specific outputs of interest; and (c) offline/online computational procedures — stratagems which decouple the generation and projection stages of the approximation process. The operation count for the online stage — in which, given a new parameter value, we calculate the output of interest and associated error bound — depends only on N (typically very small) and the parametric complexity of the problem. The method is thus particularly well-suited to many-query or real-time contexts.

The RB method can readily serve in the regularization and Bayesian frameworks. However, the speed of the RB method can also serve to consider alternative techniques (assuming adequate experimental characterization) for uncertainty quantification. In this paper, we develop such a numerical approach to parameter estimation for linear parabolic PDEs.

We first formulate the parameter estimation problem: identification of the

compact set (the “uncertainty region”) of all possible parameter values consistent with experimental measurements given in the form of intervals. We then replace the true outputs with the corresponding RB output bounds to obtain a modified uncertainty region which sharply contains the true uncertainty region yet is several orders of magnitude less expensive to interrogate. Finally, we propose efficient algorithms for the construction of engineering approximations to the modified uncertainty region: from less rigorous and very fast — for initial design — to fully rigorous and less fast — for final confirmation.

The uncertainty regions contain the many possible parameter vectors consistent with the experimental data, and hence implicitly reflect well-posedness/ill-posedness. For *identifiable* [5] inverse problems, the uncertainty regions will contain and shrink to the actual unknown parameter vector as the measurement error is decreased; our method can determine uncertainty/sensitivities to numerical and experimental error, and facilitate the design of effective procedures as regards the location/number of sensors. For *non-identifiable* [5] inverse problems, the uncertainty regions are very large (or even unbounded) relative to the measurement error; our method can signal if a problem/protocol is non-identifiable, however the problem must then be treated by other (e.g., regularization) techniques. In summary, our approach is intended to confirm and characterize identifiable/well-posed problems with relatively few parameters.

This paper is organized as follows. In Section 2, we review the RB approximation and *a posteriori* error estimation techniques for linear parabolic PDEs with affine parameter dependence first introduced in [13]. In Section 3, we develop our “uncertainty region” parameter estimation procedure. In Section 4, we present numerical results for a nondestructive evaluation problem in delamination.

2. Forward Problem

2.1. Abstract Formulation

We first consider the “exact” (superscript e) *forward* problem: Given a parameter vector $\mu \in \mathcal{D} \subset \mathbf{R}^P$, we evaluate the (here, single) output of interest

$$s^e(\mu, t^k) = \ell(y^e(\mu, t^k)), \quad \forall k \in \mathbb{K}, \quad (1)$$

where the field variable, $y^e(\mu, t^k) \in Y^e$ satisfies the weak form of the μ -parametrized linear time-invariant parabolic PDE

$$\begin{aligned} m(y^e(\mu, t^k), v; \mu) + \Delta t a(y^e(\mu, t^k), v; \mu) &= m(y^e(\mu, t^{k-1}), v; \mu) \\ &+ \Delta t b(v; \mu), \quad \forall v \in Y^e, \quad \forall k \in \mathbb{K}, \end{aligned} \quad (2)$$

with initial condition (say) $y^e(\mu, t^0) = y_0(\mu) = 0$. Note for simplicity we directly consider the Euler-Backward time integration scheme for the underlying PDE over the time interval $]0, t_f]$: we divided $[0, t_f]$ into K subintervals of equal length $\Delta t = \frac{t_f}{K}$ and defined $t^k \equiv k\Delta t$, $0 \leq k \leq K$, $\mathbb{T} \equiv \{t^0, \dots, t^k\}$, and $\mathbb{K} \equiv \{1, \dots, K\}$.

Here μ and \mathcal{D} are the input parameter and input parameter domain; $a(\cdot, \cdot; \mu)$ is a bilinear form defined over Y^e ; $m(\cdot, \cdot; \mu)$ is a bilinear form defined over X^e ; $b(\cdot; \mu)$ and $\ell(\cdot)$ are Y^e and X^e -continuous linear forms, respectively; and $Y^e \equiv H_0^1(\Omega)$ — or, more generally, $H_0^1(\Omega) \subset Y^e \subset H^1(\Omega)$ — and $X^e \equiv L^2(\Omega)$. Recall that $H^1(\Omega) = \{v \mid v \in L^2(\Omega), \nabla v \in (L^2(\Omega))^d\}$ and $H_0^1(\Omega) = \{v \mid v \in H^1(\Omega), v|_{\partial\Omega} = 0\}$, and that $L^2(\Omega)$ is the space of square integrable functions over Ω [27]. We associate to our Hilbert spaces Y^e (respectively, X^e) inner product and induced norm, $(w, v)_{Y^e}$ and $\|w\|_{Y^e} = \sqrt{(w, w)_{Y^e}}$ (respectively, $(w, v)_{X^e}$ and $\|w\|_{X^e} = \sqrt{(w, w)_{X^e}}$).

We next introduce a reference finite element approximation space $Y \subset Y^e (\subset X^e)$ of very large dimension \mathcal{N} ; we further define $X \equiv X^e$. Note that Y and X shall inherit the inner product and norm from Y^e and X^e , respectively. Our reference (or “truth”) approximation $y(\mu, t^k) \in Y$ to the exact problem (2) is then given by

$$\begin{aligned} m(y(\mu, t^k), v; \mu) + \Delta t a(y(\mu, t^k), v; \mu) &= m(y(\mu, t^{k-1}), v; \mu) \\ &+ \Delta t b(v; \mu), \quad \forall v \in Y, \quad \forall k \in \mathbb{K}, \end{aligned} \quad (3)$$

with initial condition $y(\mu, t^0) = 0$; we then evaluate the output $s(\mu, t^k) \in \mathbf{R}$ from

$$s(\mu, t^k) = \ell(y(\mu, t^k)), \quad \forall k \in \mathbb{K}. \quad (4)$$

We shall assume — hence the appellation “truth” — that the discretization is sufficiently rich such that $y(\mu, t^k)$ and $y^e(\mu, t^k)$ and hence $s(\mu, t^k)$ and $s^e(\mu, t^k)$ are indistinguishable. The RB approximation shall be built upon, and the RB error will thus be evaluated with respect to, our reference approximation $y(\mu, t^k) \in Y$. Clearly, our methods must remain computationally efficient and stable as $\mathcal{N} \rightarrow \infty$.

We shall make the following assumptions. First, we assume that for all $\mu \in \mathcal{D}$ the bilinear forms $a(\cdot, \cdot; \mu)$ and $m(\cdot, \cdot; \mu)$ are continuous,

$$a(w, v; \mu) \leq \gamma(\mu) \|w\|_Y \|v\|_Y \leq \gamma_0 \|w\|_Y \|v\|_Y, \quad \forall w, v \in Y, \quad (5)$$

$$m(w, v; \mu) \leq \rho(\mu) \|w\|_X \|v\|_X \leq \rho_0 \|w\|_X \|v\|_X, \quad \forall w, v \in X; \quad (6)$$

coercive,

$$0 < \alpha_0 \leq \alpha(\mu) \equiv \inf_{v \in Y} \frac{a(v, v; \mu)}{\|v\|_Y^2}, \quad (7)$$

$$0 < \sigma_0 \leq \sigma(\mu) \equiv \inf_{v \in Y} \frac{m(v, v; \mu)}{\|v\|_X^2}, \quad (8)$$

and symmetric, $a(v, w; \mu) = a(w, v; \mu)$, $\forall w, v \in Y$, and $m(v, w; \mu) = m(w, v; \mu)$, $\forall w, v \in X$. We also require that the linear forms $b(\cdot; \mu) : Y \rightarrow \mathbf{R}$ and $\ell(\cdot) : Y \rightarrow \mathbf{R}$ be bounded with respect to $\|\cdot\|_Y$ and $\|\cdot\|_X$, respectively.

Second, we shall assume that a , m , and b depend affinely on the parameter μ and can be expressed as

$$a(w, v; \mu) = \sum_{q=1}^{Q_a} \Theta_a^q(\mu) a^q(w, v), \quad \forall w, v \in Y, \quad \forall \mu \in \mathcal{D}, \quad (9)$$

$$m(w, v; \mu) = \sum_{q=1}^{Q_m} \Theta_m^q(\mu) m^q(w, v), \quad \forall w, v \in Y, \quad \forall \mu \in \mathcal{D}, \quad (10)$$

$$b(v; \mu) = \sum_{q=1}^{Q_b} \Theta_b^q(\mu) b^q(v), \quad \forall v \in Y, \quad \forall \mu \in \mathcal{D}, \quad (11)$$

for some (preferably) small integers $Q_{a,m,b}$. Here, the functions $\Theta_{a,m,b}^q(\mu) : \mathcal{D} \rightarrow \mathbf{R}$ depend on μ , but the continuous forms a^q , m^q , and b^q do *not* depend on μ . This

affine parameter dependence is crucial for the computational efficiency of the proposed method; however, see [6, 34] for extensions to the non-affine and nonlinear case.

We shall also assume two further hypotheses: first, that our functions $\Theta_{a,m,b}^q$ are $C^1(\mathcal{D})$ — the first derivatives are continuous over the parameter domain; and second, that our forms are “parametrically coercive” such that

$$\Theta_a^q(\mu) > 0, \quad \forall \mu \in \mathcal{D}, 1 \leq q \leq Q_a \quad (12)$$

$$\Theta_m^q(\mu) > 0, \quad \forall \mu \in \mathcal{D}, 1 \leq q \leq Q_m, \quad (13)$$

and

$$a^q(v, v) \geq 0, \quad \forall v \in Y, 1 \leq q \leq Q_a \quad (14)$$

$$m^q(v, v) \geq 0, \quad \forall v \in Y, 1 \leq q \leq Q_m. \quad (15)$$

These hypotheses are only required for our most rigorous uncertainty region approximation.

To ensure rapid convergence of the RB output approximation we introduce a dual (or adjoint) problem which shall evolve backward in time [8]. Invoking the linear time-invariant property we can express the adjoint for the output at time t^L , $1 \leq L \leq K$, as $\psi_L(\mu, t^k) = \Psi(\mu, t^{K-L+k})$, $1 \leq k \leq L$, where $\Psi(\mu, t^k) \in Y$ satisfies

$$m(v, \Psi(\mu, t^k); \mu) + \Delta t a(v, \Psi(\mu, t^k); \mu) = m(v, \Psi(\mu, t^{k+1}); \mu), \quad \forall v \in Y, \forall k \in \mathbb{K}, \quad (16)$$

with final condition

$$m(v, \Psi(\mu, t^{K+1}); \mu) \equiv \ell(v), \quad \forall v \in Y. \quad (17)$$

Thus, to obtain $\psi_L(\mu, t^k)$, $1 \leq k \leq L$, $\forall L \in \mathbb{K}$, we solve *once* for $\Psi(\mu, t^k)$, $\forall k \in \mathbb{K}$, and then appropriately shift the result — we do not need to solve K separate dual problems.

In actual practice (and later in this paper), we consider I outputs, $s^i(\mu, t^k)$, $1 \leq i \leq I$, and hence I corresponding output functionals, ℓ^i , and adjoints. (The method presented here also easily extends to nonzero initial conditions with affine parameter dependence, and to nonsymmetric problems such as the convection-diffusion equation [11, 13].)

2.2. RB Approximation

2.2.1. *Formulation* We first introduce the nested sample sets $S_{N_{\text{pr}}}^{\text{pr}} = \{\tilde{\mu}_1^{\text{pr}} \in \tilde{\mathcal{D}}, \dots, \tilde{\mu}_{N_{\text{pr}}}^{\text{pr}} \in \tilde{\mathcal{D}}\}$, $1 \leq N_{\text{pr}} \leq N_{\text{pr,max}}$, and $S_{N_{\text{du}}}^{\text{du}} = \{\tilde{\mu}_1^{\text{du}} \in \tilde{\mathcal{D}}, \dots, \tilde{\mu}_{N_{\text{du}}}^{\text{du}} \in \tilde{\mathcal{D}}\}$, $1 \leq N_{\text{du}} \leq N_{\text{du,max}}$, where $\tilde{\mu} \equiv (\mu, t^k)$ and $\tilde{\mathcal{D}} \equiv \mathcal{D} \times \mathbb{T}$; note that the samples must reside in the *parameter-discrete time* space, $\tilde{\mathcal{D}}$. Here, N_{pr} and N_{du} are the dimensions of the RB space for the primal and dual variables, respectively; in general, $S_{N_{\text{pr}}}^{\text{pr}} \neq S_{N_{\text{du}}}^{\text{du}}$, and in fact $N_{\text{pr}} \neq N_{\text{du}}$. We then define the associated hierarchical Lagrangian [25] RB spaces

$$W_{N_{\text{pr}}}^{\text{pr}} = \text{span}\{\zeta_n^{\text{pr}} \equiv y(\tilde{\mu}_n^{\text{pr}}), 1 \leq n \leq N_{\text{pr}}\}, \quad 1 \leq N_{\text{pr}} \leq N_{\text{pr,max}}, \quad (18)$$

and

$$W_{N_{\text{du}}}^{\text{du}} = \text{span}\{\zeta_n^{\text{du}} \equiv \Psi(\tilde{\mu}_n^{\text{du}}), 1 \leq n \leq N_{\text{du}}\}, \quad 1 \leq N_{\text{du}} \leq N_{\text{du,max}}, \quad (19)$$

where $y(\tilde{\mu}_n^{\text{pr}})$ is the solution of (3) at time $t = (t^k)_n^{\text{pr}} \equiv t^{k_n^{\text{pr}}}$ for $\mu = \mu_n^{\text{pr}}$ and $\Psi(\tilde{\mu}_n^{\text{du}})$ is the solution of (16) at time $t = (t^k)_n^{\text{du}} \equiv t^{k_n^{\text{du}}}$ for $\mu = \mu_n^{\text{du}}$. (In actual practice, the basis functions are orthogonalized [12, 23].)

Our RB approximation $y_N(\mu, t^k)$ to $y(\mu, t^k)$ is then obtained by a standard Galerkin projection: given $\mu \in \mathcal{D}$, $y_N(\mu, t^k) \in W_{N_{\text{pr}}}^{\text{pr}}$ satisfies

$$\begin{aligned} m(y_N(\mu, t^k), v; \mu) + \Delta t a(y_N(\mu, t^k), v; \mu) &= m(y_N(\mu, t^{k-1}), v; \mu) \\ &+ \Delta t b(v; \mu), \quad \forall v \in W_{N_{\text{pr}}}^{\text{pr}}, \quad \forall k \in \mathbb{K}, \end{aligned} \quad (20)$$

with initial condition $y_N(\mu, t^0) = 0$. Similarly, we obtain the RB approximation $\Psi_N(\mu, t^k) \in W_{N_{\text{du}}}^{\text{du}}$ to $\Psi(\mu, t^k)$ as the solution of

$$\begin{aligned} m(v, \Psi_N(\mu, t^k); \mu) + \Delta t a(v, \Psi_N(\mu, t^k); \mu) &= \\ m(v, \Psi_N(\mu, t^{k+1}); \mu), \quad \forall v \in W_{N_{\text{du}}}^{\text{du}}, \quad \forall k \in \mathbb{K}, \end{aligned} \quad (21)$$

with final condition

$$m(v, \Psi_N(\mu, t^{K+1}); \mu) \equiv \ell(v), \quad \forall v \in W_{N_{\text{du}}}^{\text{du}}. \quad (22)$$

Finally, we evaluate the RB output $s_N(\mu, t^k)$ (in practice, RB outputs, $s_N^i(\mu, t^k)$, $1 \leq i \leq I$) from

$$s_N(\mu, t^k) \equiv \ell(y_N(\mu, t^k)) + \sum_{k'=1}^k R^{\text{pr}}(\Psi_N(\mu, t^{K-k+k'}); \mu, t^{k'}) \Delta t, \quad \forall k \in \mathbb{K}, \quad (23)$$

where $\forall v \in Y$, $\forall k \in \mathbb{K}$,

$$R^{\text{pr}}(v; \mu, t^k) \equiv b(v; \mu) - a(y_N(\mu, t^k), v; \mu) - \frac{1}{\Delta t} m(y_N(\mu, t^k) - y_N(\mu, t^{k-1}), v; \mu), \quad (24)$$

is the primal residual; the residual correction in (23) ensures much higher output accuracy. Note that here $N \equiv (N_{\text{pr}}, N_{\text{du}})$.

The critical observation is that the field variable $y(\mu, t^k)$, $\forall k \in \mathbb{K}$, is not, in fact, some arbitrary member of the very high dimensional finite element space Y ; rather, it resides, or “evolves,” on a much lower dimensional manifold — in effect, a $P + 1$ dimensional manifold — induced by the parametric and temporal dependence. Thus, by restricting our attention to this manifold, we can adequately approximate the field variable by a space of dimension $N_{\text{pr}}, N_{\text{du}} \ll \mathcal{N}$. This observation is fundamental to our approach, and is the motivation for our approximation.

2.2.2. Computational Procedure We now develop offline-online computational procedures in order to fully exploit the dimension reduction of the problem [4, 15, 17, 26].

We first express $y_N(\mu, t^k)$ and $\Psi_N(\mu, t^k)$ as

$$y_N(\mu, t^k) = \sum_{n=1}^{N_{\text{pr}}} y_{Nn}(\mu, t^k) \zeta_n^{\text{pr}}, \quad (25)$$

and

$$\Psi_N(\mu, t^k) = \sum_{n=1}^{N_{\text{du}}} \Psi_{Nn}(\mu, t^k) \zeta_n^{\text{du}}, \quad (26)$$

respectively. We then choose as test functions $v = \zeta_n^{\text{pr}}$, $1 \leq n \leq N_{\text{pr}}$, for the primal problem (20) and $v = \zeta_n^{\text{du}}$, $1 \leq n \leq N_{\text{du}}$, for the dual problem (21).

It follows from (20) that $\underline{y}_N(\mu, t^k) = [y_{N1}(\mu, t^k) \ y_{N2}(\mu, t^k) \ \dots \ y_{N_{N_{\text{pr}}}}(\mu, t^k)]^T \in \mathbf{R}^{N_{\text{pr}}}$ satisfies

$$(M_N^{\text{pr}}(\mu) + \Delta t A_N^{\text{pr}}(\mu)) \underline{y}_N(\mu, t^k) = M_N^{\text{pr}}(\mu) \underline{y}_N(\mu, t^{k-1}) + \Delta t B_N^{\text{pr}}(\mu), \quad \forall k \in \mathbb{K}, \quad (27)$$

with initial condition $y_{Nn}(\mu, t^0) = 0$, $1 \leq n \leq N_{\text{pr}}$. Here, $M_N^{\text{pr}}(\mu) \in \mathbf{R}^{N_{\text{pr}} \times N_{\text{pr}}}$ and $A_N^{\text{pr}}(\mu) \in \mathbf{R}^{N_{\text{pr}} \times N_{\text{pr}}}$ are SPD matrices with entries $M_{Nij}^{\text{pr}}(\mu) = m(\zeta_i^{\text{pr}}, \zeta_j^{\text{pr}}; \mu)$, $1 \leq i, j \leq N_{\text{pr}}$, and $A_{Nij}^{\text{pr}}(\mu) = a(\zeta_i^{\text{pr}}, \zeta_j^{\text{pr}}; \mu)$, $1 \leq i, j \leq N_{\text{pr}}$, respectively; and $B_N^{\text{pr}}(\mu) \in \mathbf{R}^{N_{\text{pr}}}$ is the control vector with entries $B_{Ni}^{\text{pr}}(\mu) = b(\zeta_i^{\text{pr}}; \mu)$, $1 \leq i \leq N_{\text{pr}}$.

Invoking the affine decomposition (9)-(11), we obtain

$$M_N^{\text{pr}}(\mu) = \sum_{q=1}^{Q_m} \Theta_m^q(\mu) M_N^{\text{pr}q}, A_N^{\text{pr}}(\mu) = \sum_{q=1}^{Q_a} \Theta_a^q(\mu) A_N^{\text{pr}q}, B_N^{\text{pr}}(\mu) = \sum_{q=1}^{Q_b} \Theta_b^q(\mu) B_N^{\text{pr}q}, \quad (28)$$

where the *parameter independent* quantities $M_N^{\text{pr}q} \in \mathbf{R}^{N_{\text{pr}} \times N_{\text{pr}}}$, $A_N^{\text{pr}q} \in \mathbf{R}^{N_{\text{pr}} \times N_{\text{pr}}}$, and $B_N^{\text{pr}q} \in \mathbf{R}^{N_{\text{pr}}}$ are given by

$$\begin{aligned} M_{Nij}^{\text{pr}q} &= m^q(\zeta_i^{\text{pr}}, \zeta_j^{\text{pr}}), \quad 1 \leq i, j \leq N_{\text{pr,max}}, \quad 1 \leq q \leq Q_m, \\ A_{Nij}^{\text{pr}q} &= a^q(\zeta_i^{\text{pr}}, \zeta_j^{\text{pr}}), \quad 1 \leq i, j \leq N_{\text{pr,max}}, \quad 1 \leq q \leq Q_a, \\ B_{Ni}^{\text{pr}q} &= b^q(\zeta_i^{\text{pr}}), \quad 1 \leq i \leq N_{\text{pr,max}}, \quad 1 \leq q \leq Q_b, \end{aligned} \quad (29)$$

respectively. (A similar computational procedure for the dual problem (21)-(22) and the residual correction term in (23) can also be developed. The details of this derivation and the definitions of the necessary quantities are included in [13].)

The offline-online decomposition is as follows. In the offline stage — performed only *once* — we first solve for the ζ_n^{pr} , $1 \leq n \leq N_{\text{pr,max}}$, and ζ_n^{du} , $1 \leq n \leq N_{\text{du,max}}$; we then compute and store the μ -independent quantities for the primal problem (e.g., $M_N^{\text{pr}q}$, $A_N^{\text{pr}q}$, and $B_N^{\text{pr}q}$), for the dual problem, and for the output estimate. The computational cost is therefore dependent on $N_{\text{pr,max}}$, $N_{\text{du,max}}$, and \mathcal{N} — the dimension of the “truth” finite element approximation space.

In the online stage — performed many times, for each new parameter value μ — we first assemble the RB matrices; this requires $O((N_{\text{pr}}^2 + N_{\text{du}}^2 + N_{\text{pr}}N_{\text{du}})(Q_a + Q_m))$ operations. We then solve the primal and dual problem for $\underline{y}_N(\mu, t^k)$ and $\underline{\Psi}_N(\mu, t^k)$, respectively; since the RB matrices are in general full, the operation count is $O(N_{\text{pr}}^3 + N_{\text{du}}^3 + K(N_{\text{pr}}^2 + N_{\text{du}}^2))$. Finally, given $\underline{y}_N(\mu, t^k)$ and $\underline{\Psi}_N(\mu, t^k)$ we evaluate the output estimate $s_N(\mu, t^k)$ at a cost of $O(2kN_{\text{pr}}N_{\text{du}})$; note that the calculation of all outputs $s_N(\mu, t^k)$, $\forall k \in \mathbb{K}$, requires $O(K(K+1)N_{\text{pr}}N_{\text{du}})$ operations. Thus, as required in the many-query or real-time contexts, the online complexity is *independent* of \mathcal{N} . Since

$N_{\text{pr}}, N_{\text{du}} \ll \mathcal{N}$ we expect significant computational savings in the online stage relative to classical discretization and solution approaches.

2.3. A Posteriori Error Estimation

In order to be certain that our RB approximation satisfies the accuracy level of interest — and does not introduce new unqualified errors into the inverse procedure — we must develop rigorous *a posteriori* error estimators. Indeed, as seen in the next section, the reliability and efficiency of our parameter estimation procedure rests crucially on the *a posteriori* bounds for the error $|s(\mu, t^k) - s_N(\mu, t^k)|$: the *a posteriori* error bounds will not only eliminate (numerical) uncertainty introduced by the RB approximation, but also allow us to choose *minimal* — and hence most efficient — N_{pr} and N_{du} while satisfying the required accuracy.

2.3.1. Preliminaries To begin, we assume that we are given positive lower bounds for the coercivity constants, $\alpha(\mu)$ and $\sigma(\mu)$: $\hat{\alpha}(\mu) : \mathcal{D} \rightarrow \mathbf{R}_+$ satisfies

$$\alpha(\mu) \geq \hat{\alpha}(\mu) \geq \hat{\alpha}_0 > 0, \quad \forall \mu \in \mathcal{D}, \quad (30)$$

and $\hat{\sigma}(\mu) : \mathcal{D} \rightarrow \mathbf{R}_+$ satisfies

$$\sigma(\mu) \geq \hat{\sigma}(\mu) \geq \hat{\sigma}_0 > 0, \quad \forall \mu \in \mathcal{D}; \quad (31)$$

various recipes for this construction can be found in [13, 23, 26, 35]. We next specify the inner products

$$(v, w)_Y \equiv a(v, w; \mu_{\text{ref}}), \quad \forall v, w \in Y, \quad (32)$$

and

$$(v, w)_X \equiv m(v, w; \mu_{\text{ref}}), \quad \forall v, w \in Y, \quad (33)$$

for some constant reference value μ_{ref} . Recall also that $\|\cdot\|_Y = (\cdot, \cdot)_Y^{1/2}$, $\|\cdot\|_X = (\cdot, \cdot)_X^{1/2}$.

We now introduce the dual norm of the primal residual

$$\varepsilon_{N_{\text{pr}}}^{\text{pr}}(\mu, t^k) \equiv \sup_{v \in Y} \frac{R^{\text{pr}}(v; \mu, t^k)}{\|v\|_Y}, \quad \forall k \in \mathbb{K}, \quad (34)$$

and the dual norm of the dual residual

$$\varepsilon_{N_{\text{du}}}^{\text{du}}(\mu, t^k) \equiv \sup_{v \in Y} \frac{R^{\text{du}}(v; \mu, t^k)}{\|v\|_Y}, \quad \forall k \in \mathbb{K}, \quad (35)$$

where for all $v \in Y$ and $k \in \mathbb{K}$,

$$R^{\text{du}}(v; \mu, t^k) \equiv -a(v, \Psi_N(\mu, t^k); \mu) - \frac{1}{\Delta t} m(v, \Psi_N(\mu, t^k) - \Psi_N(\mu, t^{k+1}); \mu), \quad (36)$$

is the dual residual. We also define the dual norm

$$\varepsilon_{N_{\text{du}}}^{\Psi_f}(\mu) \equiv \sup_{v \in Y} \frac{R^{\Psi_f}(v; \mu)}{\|v\|_X}, \quad (37)$$

where

$$R^{\Psi_f}(v; \mu) = \ell(v) - m(v, \Psi_N(\mu, t^{K+1}); \mu), \quad \forall v \in Y, \quad (38)$$

is the residual for the final condition (17).

2.3.2. Output Bounds Finally, we present the *a posteriori* error estimation results for the error in the output estimate, and refer to [13] for the proof.

Proposition 2.1. *For the output of interest, $s(\mu, t^k)$ in (4), and the RB output estimate, $s_N(\mu, t^k)$ in (23), the error in the output of interest is bounded by*

$$|s(\mu, t^k) - s_N(\mu, t^k)| \leq \Delta_N^s(\mu, t^k), \quad \forall \mu \in \mathcal{D}, \quad \forall k \in \mathbb{K}, \quad (39)$$

where the output bound $\Delta_N^s(\mu, t^k)$ is defined as

$$\Delta_N^s(\mu, t^k) \equiv \Delta_{N_{\text{pr}}}^{\text{pr}}(\mu, t^k) \Delta_{N_{\text{du}}}^{\text{du}}(\mu, t^{K-k+1}), \quad (40)$$

with

$$\Delta_{N_{\text{pr}}}^{\text{pr}}(\mu, t^k) \equiv \left(\frac{\Delta t}{\hat{\alpha}(\mu)} \sum_{k'=1}^k \varepsilon_{N_{\text{pr}}}^{\text{pr}}(\mu, t^{k'})^2 \right)^{\frac{1}{2}}, \quad (41)$$

$$\Delta_{N_{\text{du}}}^{\text{du}}(\mu, t^k) \equiv \left(\frac{\Delta t}{\hat{\alpha}(\mu)} \sum_{k'=k}^K \varepsilon_{N_{\text{du}}}^{\text{du}}(\mu, t^{k'})^2 + \frac{\varepsilon_{N_{\text{du}}}^{\Psi_f}(\mu)^2}{\hat{\sigma}(\mu)} \right)^{\frac{1}{2}}. \quad (42)$$

Here $\Delta_{N_{\text{pr}}}^{\text{pr}}(\mu, t^k)$ and $\Delta_{N_{\text{du}}}^{\text{du}}(\mu, t^k)$ are the error estimates for the errors in the primal variable and the dual variable, respectively.

In actual practice, we compute an error bound $\Delta_N^i(\mu, t^k)$ for each RB output $s_N^i(\mu, t^k)$, $1 \leq i \leq I$.

2.3.3. Computational Procedure The offline-online computational procedures for the calculation of $\Delta_{N_{\text{pr}}}^{\text{pr}}(\mu, t^k)$, $\Delta_{N_{\text{du}}}^{\text{du}}(\mu, t^k)$, and $\Delta^s(\mu, t^k)$ are rather long; we refer the reader to [13] for a detailed implementation. Here, we only summarize the computational costs involved.

The computational cost in the offline stage is (to leading order) $O((N_{\text{pr,max}} + N_{\text{du,max}})(Q_a + Q_m))$ solutions of the underlying “truth” finite element approximation and $O((N_{\text{pr,max}}^2 + N_{\text{du,max}}^2)(Q_a^2 + Q_a Q_m + Q_m^2))$ \mathcal{N} -inner products; the storage requirement is $O((N_{\text{pr,max}}^2 + N_{\text{du,max}}^2)(Q_a^2 + Q_a Q_m + Q_m^2))$. In the online stage — given a new parameter value μ and associated RB solutions $\underline{y}_N(\mu, t^k)$ and $\underline{\Psi}_N(\mu, t^k)$, $\forall k \in \mathbb{K}$ — the computational cost to evaluate $\Delta^s(\mu, t^k)$, $\forall k \in \mathbb{K}$, is $O(K(N_{\text{pr}}^2 + N_{\text{du}}^2)(Q_a^2 + Q_a Q_m + Q_m^2))$; for multiple outputs the effort scales as I . Thus, all online calculations needed are *independent* of \mathcal{N} and hence very fast.

3. Parameter Estimation Procedures

In this section, we apply our RB output bound method to reliable real-time parameter estimation for linear parabolic (parametrically coercive) PDEs with affine parameter dependence. We emphasize that the following development is not restricted to linear parabolic PDEs, but in general can be extended to various types of PDEs provided that the RB approximation and *a posteriori* error bounds for functional outputs are available.

3.1. Formulation of Parameter Estimation Problems

Reconciliation of output predictions and experimental measurements — each with their own uncertainty — form the basis for formulating a parameter estimation problem. In the presence of data uncertainty, formulation of parameter estimation problems depends on many factors such as the nature of the forward problem, the uncertainty level in the measurements, and the way in which the experimental uncertainty is characterized. The present formulation is useful when information on the experimental measurements are available as bounds in the form of intervals.

We assume that there are I different measured outputs g^i , $1 \leq i \leq I$, each of which is

measured at J different time levels $t_j^{k_{\text{exp}}}$, $1 \leq j \leq J$, where $\mathbb{K}_{\text{exp}} = \{k_1^{\text{exp}}, \dots, k_J^{\text{exp}}\} \subset \mathbb{K}$; the measurements can be summarized as a matrix quantity $G \in \mathbf{R}^{I \times J}$ with entries $G_{ij} = g^i(t_j^{k_{\text{exp}}})$, $1 \leq i \leq I, 1 \leq j \leq J$. We further assume that we do not have access to the exact measurements G_{ij} , but that lower bounds G_{ij}^L and upper bounds G_{ij}^U are *known* such that

$$G_{ij}^L \leq G_{ij} \leq G_{ij}^U, \quad 1 \leq i \leq I, 1 \leq j \leq J. \quad (43)$$

We also define $s^i(\mu, t^k)$, $1 \leq i \leq I, 1 \leq k \leq K$, as the truth approximation outputs corresponding to the measured quantities: $s^i(\mu^*, t_j^{k_{\text{exp}}}) = g^i(t_j^{k_{\text{exp}}})$, $1 \leq i \leq I, 1 \leq j \leq J$, for the actual (but unknown) value of the parameter $\mu^* \in \mathcal{D}$. Recall that we assume that our truth solution is indistinguishable from the exact solution — which is here further assumed to be indistinguishable from the actual physical system.

We now formulate our parameter estimation problem: given the interval bounds on the exact measurements, $[G_{ij}^L, G_{ij}^U]$, $1 \leq i \leq I, 1 \leq j \leq J$, we define the *uncertainty region* as

$$\mathcal{P} = \left\{ \mu \in \mathcal{D} \mid s^i(\mu, t_j^{k_{\text{exp}}}) \in [G_{ij}^L, G_{ij}^U], 1 \leq i \leq I, 1 \leq j \leq J \right\}. \quad (44)$$

In words, we find all possible parameter values in the (possibly large) bounded parameter set \mathcal{D} that are consistent with the interval measurements $[G_{ij}^L, G_{ij}^U]$. (In fact, μ^* need not be in \mathcal{D} ; in this case, however, $\mathcal{P} = \mathcal{D}$ — a useful indicator but not a useful parameter prediction.)

Numerical methods for the construction of the uncertainty region \mathcal{P} would require the *repeated* solution of the forward problem for $s^i(\mu, t_j^{k_{\text{exp}}})$. Unfortunately, the computation of the truth approximation outputs is typically sufficiently expensive that the uncertainty region \mathcal{P} can not possibly be constructed, let alone constructed in real-time.

3.2. Formulation via RB Output Bounds

In order to achieve results (in real-time), we employ the RB output bound method described in the previous section. Towards this end, we introduce $s_N^i(\mu, t^k)$ and

$\Delta_N^{s^i}(\mu, t^k)$, $1 \leq i \leq I, 1 \leq k \leq K$, as the RB approximations and *a posteriori* error bounds corresponding to $s^i(\mu, t^k)$, $1 \leq i \leq I, 1 \leq k \leq K$. We define the RB output bounds as

$$s_N^{i\pm}(\mu, t^k) \equiv s_N^i(\mu, t^k) \pm \Delta_N^{s^i}(\mu, t^k), \quad 1 \leq i \leq I, 1 \leq k \leq K. \quad (45)$$

We may now define our modified uncertainty region

$$\mathcal{P}_N \equiv \left\{ \mu \in \mathcal{D} \mid [s_N^{i-}(\mu, t_j^{k_{\text{exp}}}), s_N^{i+}(\mu, t_j^{k_{\text{exp}}})] \cap [G_{ij}^L, G_{ij}^U] \neq \emptyset, 1 \leq i \leq I, 1 \leq j \leq J \right\}. \quad (46)$$

We also define \mathcal{E}_N as the smallest area ellipsoid that contains \mathcal{P}_N , and \mathcal{B}_N as the smallest P -piped (aligned with the parameter coordinates) that contains \mathcal{P}_N : \mathcal{E}_N and \mathcal{B}_N are often more practical than \mathcal{P}_N in engineering analyses.

We can then prove that, thanks to our RB output bounds, \mathcal{P}_N is *conservative*:

Proposition 3.1. *For \mathcal{P} and \mathcal{P}_N defined in (44) and (46), respectively, $\mathcal{P} \subset \mathcal{P}_N$ (and $\mathcal{P} \subset \mathcal{E}_N$, $\mathcal{P} \subset \mathcal{B}_N$).*

Proof. For any $\mu \in \mathcal{P}$, we note from (44) that $s^i(\mu, t_j^{k_{\text{exp}}}) \in [G_{ij}^L, G_{ij}^U]$; furthermore, we note from Proposition 2.1 that $s^i(\mu, t^k) \in [s_N^{i-}(\mu, t^k), s_N^{i+}(\mu, t^k)]$. Hence, $[s_N^{i-}(\mu, t_j^{k_{\text{exp}}}), s_N^{i+}(\mu, t_j^{k_{\text{exp}}})] \cap [G_{ij}^L, G_{ij}^U] \neq \emptyset$ which in turn implies from (46) that $\mu \in \mathcal{P}_N$. Since $\mathcal{P}_N \subset \mathcal{E}_N$, $\mathcal{P}_N \subset \mathcal{B}_N$, it immediately follows that $\mathcal{P} \subset \mathcal{E}_N$, $\mathcal{P} \subset \mathcal{B}_N$. \square

This result contains several useful and practical implications. First, if \mathcal{P}_N is an empty set then we know that something is “wrong” with our assumptions: either the mathematical model for the forward problem is not correct, or the truth approximation is inadequate, or the experimental data (43) are suspect. Second, if \mathcal{P}_N is not empty but very large compared to the intervals $[G_{ij}^L, G_{ij}^U]$ then the parameter estimation problem is *non-identifiable* [5] due to factors such as inadequate measurements. Third, if \mathcal{P}_N is a bounded region of size commensurate with, and scaling as, the intervals $[G_{ij}^L, G_{ij}^U]$, then we know that the forward modeling is correct, the truth approximation is adequate, and the collected measurements are effective: the problem is identifiable, and our approach returns a conservative estimate of the true parameter.

Fourth (turning to numerical issues), the size of \mathcal{P}_N relative to \mathcal{P} depends critically on $\Delta_N^{s^i}(\mu, t^k)$: as N increases, \mathcal{P}_N shrinks (“from above”) to \mathcal{P} ; in practice, we expect

that \mathcal{P}_N approaches \mathcal{P} quickly, since $\Delta_N^{s^i}(\mu, t^k)$ vanishes very rapidly with N . Fifth, for given $\mu \in \mathcal{D}$, the determination $\mu \in \mathcal{P}_N$ (or $\mu \notin \mathcal{P}_N$) — the basis for construction of approximations to \mathcal{P}_N (and \mathcal{E}_N and \mathcal{B}_N) — is much less expensive than the determination $\mu \in \mathcal{P}$ (or $\mu \notin \mathcal{P}$): the RB output bounds $s_N^{i\pm}(\mu, t^k)$ are several orders of magnitude less costly than direct calculation of the truth approximation outputs $s^i(\mu, t^k)$, and hence \mathcal{P}_N can be much more readily interrogated than \mathcal{P} .

3.3. Approximate Bounding Regions

Exact construction of the regions \mathcal{P}_N , \mathcal{E}_N , \mathcal{B}_N is not possible in finite time, let alone in real-time, even with the rapid RB evaluations. We thus consider approximations to these regions. The first three approximations $\tilde{\mathcal{P}}_N$, $\tilde{\mathcal{E}}_N$, and $\tilde{\mathcal{B}}_N$ are very fast but not, in general, rigorous: we can not prove $\mathcal{P} \subset \tilde{\mathcal{P}}_N$, $\mathcal{P} \subset \tilde{\mathcal{E}}_N$, or $\mathcal{P} \subset \tilde{\mathcal{B}}_N$. The last approximation \mathcal{R}_N is less fast but rigorous: we can prove $\mathcal{P} \subset \mathcal{R}_N$.

We develop an offline-online procedure for the construction of these approximations. In the offline stage — performed only once — we compute and store the μ -independent quantities for both the primal problem and I adjoint problems. The offline stage is computationally extensive and performed only once — more precisely, each time we wish to change the outputs or consider a new output. In the online stage — for the given experimental measurements $[G_{ij}^L, G_{ij}^U], 1 \leq i \leq I, 1 \leq j \leq J$, and RB dimension N — we pursue the algorithms given below for the construction of $\tilde{\mathcal{P}}_N$, $\tilde{\mathcal{E}}_N$, $\tilde{\mathcal{B}}_N$, and \mathcal{R}_N . The offline cost can thus be amortized over *many* forward evaluations necessary for the construction of these regions, and also typically over many different values of the estimated parameter μ^* .

3.3.1. Approximate Uncertainty Region $\tilde{\mathcal{P}}_N$ We first find a $\mu_{\text{IC}} \in \mathcal{P}_N$ (which we shall call the *initial center*) from

$$\mu_{\text{IC}} = \arg \min_{\mu \in \mathcal{P}_N} \sum_{i=1}^I \sum_{j=1}^J (s_N^i(\mu, t^{k_j^{\text{exp}}}) - G_{ij}^C)^2. \quad (47)$$

Here $G_{ij}^C = 0.5(G_{ij}^L + G_{ij}^U)$ are the centers of the intervals $[G_{ij}^L, G_{ij}^U]$, $1 \leq i \leq I, 1 \leq j \leq J$. This constrained least-squares problem can be solved efficiently by a finite difference Levenberg-Marquardt algorithm [19]. (In practice, we may prefer to solve an unconstrained minimization and verify whether the minimizer satisfies the constraint.)

Next we find a set of M boundary points $\{\hat{\mu}_1, \dots, \hat{\mu}_M\}$ of \mathcal{P}_N by pursuing a binary chop search as follows. For a given angle d from the initial center μ_{IC} , we find $\mu_{out} = \mu_{IC} + \lambda d \notin \mathcal{P}_N$, and set $\mu_{in} = \mu_{IC}$ and $\hat{\mu} = 0.5(\mu_{in} + \mu_{out})$; we then repeatedly set $\mu_{in} = \hat{\mu}$ if $\hat{\mu} \in \mathcal{P}_N$ else $\mu_{out} = \hat{\mu}$, and $\hat{\mu} = 0.5(\mu_{in} + \mu_{out})$; we terminate when the distance between μ_{in} and μ_{out} is sufficiently small. It should be noted from (46) that a verification of $\hat{\mu} \in \mathcal{P}_N$ requires computation of $s_N^{i\pm}(\hat{\mu}, t_j^{k_{exp}})$, $1 \leq i \leq I, 1 \leq j \leq J$.

Finally, we define $\tilde{\mathcal{P}}_N$ to be the convex hull of these boundary points. If \mathcal{P}_N is convex (or more generally, star-shaped with respect to μ_{IC}) — hypotheses plausibly satisfied for identifiable problems in the limit of small experimental noise — then $\tilde{\mathcal{P}}_N \rightarrow \mathcal{P}_N$ as $M \rightarrow \infty$.

3.3.2. Approximate Bounding Ellipsoid $\tilde{\mathcal{E}}_N$ We construct our approximation to the bounding ellipsoid \mathcal{E}_N of \mathcal{P}_N as the bounding ellipsoid of the approximate uncertainty region $\tilde{\mathcal{P}}_N$. The problem of constructing a smallest volume ellipsoid $\tilde{\mathcal{E}}_N$ containing $\tilde{\mathcal{P}}_N$ can be solved efficiently by semi-definite programming methods [22, 32]. If $\tilde{\mathcal{P}}_N \rightarrow \mathcal{P}_N$ then $\tilde{\mathcal{E}}_N \rightarrow \mathcal{E}_N$ in the limit $M \rightarrow \infty$.

3.3.3. Approximate Bounding Box $\tilde{\mathcal{B}}_N$ We recall that our bounding box for \mathcal{P}_N is defined as

$$\mathcal{B}_N \equiv \prod_{p=1}^P [B_{\min,N}^p, B_{\max,N}^p] , \quad (48)$$

where for $p = 1, \dots, P$,

$$B_{\min,N}^p = \min_{\mu \in \mathcal{P}_N} \mu^p, \quad B_{\max,N}^p = \max_{\mu \in \mathcal{P}_N} \mu^p ; \quad (49)$$

note that $\mu = (\mu^1, \dots, \mu^P)$. Hence, we need to solve $2P$ constrained minimization and maximization problems to form \mathcal{B}_N . Our optimization shall be approximate: the

resulting approximate bounding box $\tilde{\mathcal{B}}_N$ is thus given by

$$\tilde{\mathcal{B}}_N \equiv \prod_{p=1}^P \left[\tilde{B}_{\min,N}^p, \tilde{B}_{\max,N}^p \right]. \quad (50)$$

where $\tilde{B}_{\min,N}^p$ and $\tilde{B}_{\max,N}^p$, $1 \leq p \leq P$, are our approximations to $B_{\min,N}^p$ and $B_{\max,N}^p$.

Solution of such minimization and maximization problems by trust-region interior-point methods is discussed in [24]. However, by noting that the objectives are monotonic and hence that the optimal solutions lie on the boundary of \mathcal{P}_N , we devise a very simple algorithm for solving our particular problems (49). We describe our algorithm for solving $\min_{\mu \in \mathcal{P}_N} \mu^1$; a similar procedure can be applied for the other problems.

First, we start with the initial center μ_{IC} and pursue the binary chop search along a “selected” direction to find a boundary point $\hat{\mu}$ such that $\hat{\mu}^1 < \hat{\mu}_{IC}^1$. At this boundary point, we follow a new selected direction to find a new boundary point $\hat{\mu}_{\text{new}}$ such that $\hat{\mu}_{\text{new}}^1 < \hat{\mu}^1$. (We try many feasible descent directions at $\hat{\mu}$ and select among them the direction that maximizes $\hat{\mu}^1 - \hat{\mu}_{\text{new}}^1$. Note that a direction at $\hat{\mu}$ is said to be *feasible* if there exists an interior point, and is *descent* if the objective is improved when we follow that direction.) We next set $\hat{\mu} = \hat{\mu}_{\text{new}}$ and repeat the second step until we reach a boundary point $\hat{\mu}_{\text{new}}$ at which there is no feasible descent direction to follow. Finally, we set $\tilde{B}_{\min,N}^1 = \hat{\mu}_{\text{new}}^1$.

Clearly, for \mathcal{P}_N convex, $\tilde{\mathcal{B}}_N$ will converge to \mathcal{B}_N as we refine our search directions. However, if \mathcal{P}_N is not convex, there is no such guarantee. (In some sense, convexity and μ_{IC} serve as weak “regularization” or “prior information” for this particular construction.)

3.3.4. Rigorous Bounding Region We also develop an approach, based on bounds for the sensitivity of the outputs, to provide an approximate uncertainty region \mathcal{R}_N such that $\mathcal{P} \subset \mathcal{R}_N$ is guaranteed even for \mathcal{P} *non-convex* and *non-connected*. (Note that we do not necessarily obtain $\mathcal{P}_N \subset \mathcal{R}_N$.) Recall that, for this approach, we enlist not only the assumptions (5)-(11), but also the assumption of $C^1(\mathcal{D})$ continuity of the $\Theta_{a,m,b}^q$ and parametric coercivity of the $\Theta_{a,m}^q$ and a^q, m^q . Under these assumptions, we can

construct \mathcal{R}_N as follows.

We first introduce a set of parameter points $\bar{\mu}_m, 1 \leq m \leq M$, and associated closed cells $\mathcal{C}^{\bar{\mu}_m}, 1 \leq m \leq M$, such that $\bar{\mu}_m \in \mathcal{C}^{\bar{\mu}_m}, 1 \leq m \leq M, \mathring{\mathcal{C}}^{\bar{\mu}_m} \cap \mathring{\mathcal{C}}^{\bar{\mu}_{m'}} = \emptyset, 1 \leq m < m' \leq M$, and

$$\mathcal{D} = \bigcup_{m=1}^M \mathcal{C}^{\bar{\mu}_m}. \quad (51)$$

We define \mathcal{R}_N in terms of a characteristic, or indicator, function $\chi(m) : \{1, \dots, M\} \rightarrow \{0, 1\}$:

$$\mathcal{R}_N = \bigcup_{\{m \in \{1, \dots, M\} \mid \chi(m)=1\}} \mathcal{C}^{\bar{\mu}_m}. \quad (52)$$

In words, $\chi(m) = 1$ (respectively, 0) indicates that the cell $\mathcal{C}^{\bar{\mu}_m}$ is in (respectively, is not in) the uncertainty region \mathcal{R}_N .

We now define our characteristic function: for $m \in \{1, \dots, M\}$,

$$\chi(m) = \begin{cases} 1, & [s_N^{i-}(\bar{\mu}_m, t^{k_j^{\text{exp}}}) - \nabla s^i(\bar{\mu}_m, t^{k_j^{\text{exp}}})\delta_m, \\ & s_N^{i+}(\bar{\mu}_m, t^{k_j^{\text{exp}}}) + \nabla s^i(\bar{\mu}_m, t^{k_j^{\text{exp}}})\delta_m] \cap \\ & [G_{ij}^L, G_{ij}^U] \neq \emptyset, \quad 1 \leq i \leq I, 1 \leq j \leq J \\ 0, & \text{otherwise} \end{cases} \quad (53)$$

where δ_m is the *maximum* distance from $\bar{\mu}_m$ to all points in the cell $\mathcal{C}^{\bar{\mu}_m}$, and

$$\nabla s^i(\bar{\mu}_m, t^{k_j^{\text{exp}}}) = \|\ell^i\|_{X'} \sqrt{\sum_{p=1}^P \left(\nabla_y^p(\bar{\mu}_m, t^{k_j^{\text{exp}}}) \right)^2}. \quad (54)$$

Here, for any $\bar{\mu}$ and $\mathcal{C}^{\bar{\mu}}, \nabla_y^p(\bar{\mu}, t^k), 1 \leq p \leq P$, is given by

$$\begin{aligned} \nabla_y^p(\bar{\mu}, t^k) = \max_{\mu \in \mathcal{C}^{\bar{\mu}_m}} & \left\{ 2k\Delta t \left(\frac{2\Upsilon_m^p(\mu) + \Upsilon_a^p(\mu)}{\hat{\alpha}(\mu)\hat{\sigma}(\mu)} \right) \left(\sum_{q=1}^{Q_b} \Theta_b^q(\mu) \|b^q\|_{Y'} \right)^2 \right. \\ & \left. + \frac{2k\Delta t}{\hat{\alpha}(\mu)\hat{\sigma}(\mu)} \left(\sum_{q=1}^{Q_b} \left| \frac{\partial \Theta_b^q(\mu)}{\partial \mu^p} \right| \|b^q\|_{Y'} \right)^2 \right\}^{1/2} \end{aligned} \quad (55)$$

where

$$\Upsilon_a^p(\mu) = \max_{1 \leq q \leq Q_a} \frac{(\frac{\partial \Theta_a^q(\mu)}{\partial \mu^p})^2}{(\Theta_a^q(\mu))^2}, \quad \Upsilon_m^p(\mu) = \max_{1 \leq q \leq Q_m} \frac{(\frac{\partial \Theta_m^q(\mu)}{\partial \mu^p})^2}{(\Theta_m^q(\mu))^2}, \quad (56)$$

and $\hat{\alpha}(\mu), \hat{\sigma}(\mu)$ are the lower bounds for $\alpha(\mu), \sigma(\mu)$, respectively.

We note that the determination of $\chi(m)$ requires us to compute $s_N^i(\bar{\mu}_m, t^{k_j^{\text{exp}}}), \Delta_N^i(\bar{\mu}_m, t^{k_j^{\text{exp}}})$, and $\nabla s^i(\bar{\mu}_m, t^{k_j^{\text{exp}}}), 1 \leq i \leq I, 1 \leq j \leq J$, in the online (real-time

parameter estimation) stage . (The dual norms $\|\ell^i\|_{X'}$, $1 \leq i \leq I$, and $\|b^q\|_{Y'}$, $1 \leq q \leq Q_b$, are precomputed offline.) In general, $\nabla s^i(\bar{\mu}_m, t_j^{k_{\text{exp}}})$ is less expensive than $s_N^i(\bar{\mu}_m, t_j^{k_{\text{exp}}})$ and $\Delta_N^i(\bar{\mu}_m, t_j^{k_{\text{exp}}})$. Note furthermore that for our example in the next section, and in practice quite often, the $\Theta_{a,b,m}^q(\mu)$ have very simple forms such that the maximization over $\mathcal{C}^{\bar{\mu}}$ in (55) can be performed analytically.

Proposition 3.2. *For \mathcal{P} and \mathcal{R}_N defined in (44) and (52), respectively, $\mathcal{P} \subset \mathcal{R}_N$.*

Proof. We consider a cell $\mathcal{C}^{\bar{\mu}}$ of diameter δ and apply the fundamental theorem of calculus to obtain

$$s^i(\bar{\mu}, t^k) - ds^i(\bar{\mu}, t^k)\delta \leq s^i(\mu, t^k) \leq s^i(\bar{\mu}, t^k) + ds^i(\bar{\mu}, t^k)\delta, \quad \forall \mu \in \mathcal{C}^{\bar{\mu}}, \quad (57)$$

where

$$ds^i(\bar{\mu}, t^k) = \max_{\mu \in \mathcal{C}^{\bar{\mu}}} \left\{ \sum_{p=1}^P \left(\frac{\partial s^i(\mu, t^k)}{\partial \mu^p} \right)^2 \right\}^{1/2}. \quad (58)$$

We then note that

$$\max_{\mu \in \mathcal{C}^{\bar{\mu}}} \left| \frac{\partial s^i(\mu, t^k)}{\partial \mu^p} \right| = \max_{\mu \in \mathcal{C}^{\bar{\mu}}} \left| \ell^i \left(\frac{\partial y(\mu, t^k)}{\partial \mu^p} \right) \right| \leq \|\ell^i\|_{X'} \max_{\mu \in \mathcal{C}^{\bar{\mu}}} \left\| \frac{\partial y(\mu, t^k)}{\partial \mu^p} \right\|_X. \quad (59)$$

Furthermore, it follows from Proposition A.3 (from the Appendix A) and the coercivity condition (8) that

$$\begin{aligned} \left\| \frac{\partial y(\mu, t^k)}{\partial \mu^p} \right\|_X^2 &\leq 2k\Delta t \left(\frac{2\Upsilon_m^p(\mu) + \Upsilon_a^p(\mu)}{\hat{\alpha}(\mu)\hat{\sigma}(\mu)} \right) \|b(\cdot; \mu)\|_{Y'}^2 + \frac{2k\Delta t}{\hat{\alpha}(\mu)\hat{\sigma}(\mu)} \left\| \frac{\partial b(\cdot; \mu)}{\partial \mu^p} \right\|_{Y'}^2 \\ &\leq 2k\Delta t \left(\frac{2\Upsilon_m^p(\mu) + \Upsilon_a^p(\mu)}{\hat{\alpha}(\mu)\hat{\sigma}(\mu)} \right) \left(\sum_{q=1}^{Q_b} \Theta_b^q(\mu) \|b^q\|_{Y'} \right)^2 \\ &\quad + \frac{2k\Delta t}{\hat{\alpha}(\mu)\hat{\sigma}(\mu)} \left(\sum_{q=1}^{Q_b} \left| \frac{\partial \Theta_b^q(\mu)}{\partial \mu^p} \right| \|b^q\|_{Y'} \right)^2 \end{aligned} \quad (60)$$

which, after taking the max over $\mathcal{C}^{\bar{\mu}}$ for both sides, gives

$$\max_{\mu \in \mathcal{C}^{\bar{\mu}}} \left\| \frac{\partial y(\mu, t^k)}{\partial \mu^p} \right\|_X \leq \nabla_y^p(\bar{\mu}_m, t^k), \quad \forall \mu \in \mathcal{C}^{\bar{\mu}}. \quad (61)$$

We thus have from (58), (59), (54), (55), and (61) that

$$ds^i(\bar{\mu}, t^k) \leq \nabla s^i(\bar{\mu}, t^k). \quad (62)$$

We can now assemble the final result.

It follows from (57),(62) and Proposition 2.1 that $\forall \mu \in \mathcal{C}^{\bar{\mu}}, 1 \leq k \leq K, 1 \leq i \leq I$,

$$s^i(\mu, t^k) \in [s_N^{i-}(\bar{\mu}, t^k) - \nabla s^i(\bar{\mu}, t^k)\delta, s_N^{i+}(\bar{\mu}, t^k) + \nabla s^i(\bar{\mu}, t^k)\delta]. \quad (63)$$

Furthermore, for any $\mu \in \mathcal{P}$, we note from (44) that $s^i(\mu, t_j^{k_{\text{exp}}}) \in [G_{ij}^L, G_{ij}^U], 1 \leq i \leq I, 1 \leq j \leq J$, and from (51) that there exists an $m \in \{1, \dots, M\}$ such that $\mu \in \mathcal{C}^{\bar{\mu}_m}$; thus, for any $\mu \in \mathcal{P}$, it follows from (63) (for $\bar{\mu} = \bar{\mu}_m$ and $\delta = \delta_m$) and (53) that $\chi(m) = 1$ — which in turn implies from (52) that $\mu \in \mathcal{C}^{\bar{\mu}_m} \subset \mathcal{R}_N$. This completes the proof. \square

To construct \mathcal{R}_N , we apply a simple hierarchical/divide-and-conquer strategy: we begin with the parameter domain \mathcal{D} as a single cell and set $L_{\text{ref}} = 0$; we iteratively divide each of the cells (which survive from the previous iteration) into (say) 2^P subcells and remove the $\chi(m) = 0$ subcells; we then increment L_{ref} and repeat the process. As we increase L_{ref} , \mathcal{R}_N will continue to shrink, and in particular approach \mathcal{P} as $L_{\text{ref}} \rightarrow \infty$ (and $N \rightarrow \infty$); however, the total number of evaluated cells M will of course also increase, leading to an increase in computational cost. Typically, we choose L_{ref} so that $\nabla s^i(\bar{\mu}_m, t^k)\delta_m$ is commensurate with the measurement error.

In actual practice, and even with the rapid RB response, evaluation of the characteristic function in each of the M cells will be quite prohibitive especially for multi-dimensional parameter spaces. Nevertheless, \mathcal{R}_N does provide complete rigor in the numerical quantification of the uncertainty region \mathcal{P} . Hence, although both slightly less general as developed here (due to additional assumptions on the forward problems) and certainly more computationally expensive than the proposals of the previous subsections, this inverse procedure can be gainfully employed in certain applications with a high premium on (say) safety.

4. Nondestructive Evaluation of Concrete Delamination

4.1. Problem Description

Fiber-Reinforced Polymer (FRP) composites are applied widely in civil engineering for bridge column seismic retrofits to strengthen concrete and masonry structures, as well as

in the rehabilitation of existing infrastructure [14]. To enhance the structural capacity of the design, layers of FRP composites are bonded to concrete structures using adhesives such as epoxy resins. The success and performance of this reinforcement depends strongly on the quality of the bond between the FRP composite and the substrate. Since debonds or delaminations at the composite-concrete interface often occur (even at installation), effective quality control — providing reliable information about the thickness and fiber content of the composite, and the number, location, and size of defects — is vital to safety. There is thus a need not only for the *detection* of flaws, but also for accurate *characterization* of the detected flaws, and in the field — in real-time.

Infrared (IR) thermography is a common technique for Non-Destructive Evaluation (NDE). IR thermography has been successfully applied to detect flaws in FRP composites bonded to concrete [28]: the approach is sensitive to the presence of defects near the surface and allows for the efficient investigation of large surface areas. In active IR thermography, the structure is externally heated and the surface temperature is monitored using an IR imaging system. The heat transfer in the structure is affected by the presence of flaws in the structure, which gives rise to localized hot or cold spots on the surface. The goal is then to infer the location and size of defects from the surface temperature readings. The inverse methods must thus be *reliable* (to guarantee safety) and *efficient* (to allow for characterization in the field).

A model for a FRP composite bonded to concrete similar to the model discussed in [28] is shown in Figure 1. The concrete slab (below) is of non-dimensional length 60 and thickness 10; and the FRP layer (above) is of non-dimensional length 60 and thickness 1. We assume that there exists a delamination of unknown non-dimensional width, w_{del} , located on the composite-concrete interface and centered at $x_1 = 0$. The thermal conductivity of concrete is denoted k_C , and the thermal conductivity of the FRP is denoted k_{FRP} ; while the former is assumed known (the uncertainty is very small in practice), the latter depends on the direction of the fibers and the fiber content and is less predictable. We define $\kappa \equiv k_{\text{FRP}}/k_C$ as the ratio of the two thermal conductivities.

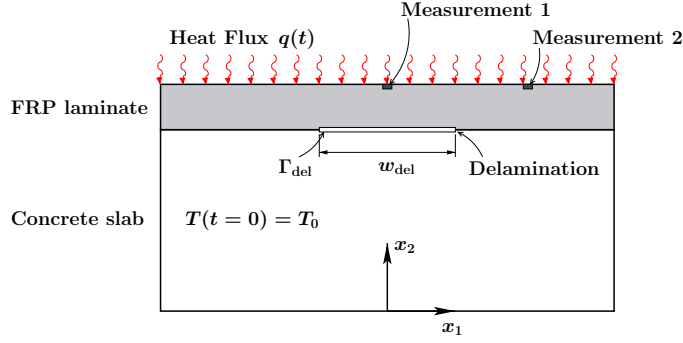


Figure 1. AP I: Delamination of FRP bonded to concrete.

We assume that the volumetric specific heats of the concrete and FRP are identical (and hence absorbed in the non-dimensional time).

The non-dimensional heat flux, $q(t) = \bar{q}(t)t_{\text{FRP}}/(k_C(\bar{T}_{\text{FRP,max}} - \bar{T}_0))$, is applied to the exposed surface of the structure, Γ_{top} , for non-dimensional time $t \in]0, 0.5]$; here, $\bar{q}(t)$ is the heat flux, \bar{T}_0 is the ambient and initial temperature, $\bar{T}_{\text{FRP,max}}$ is the maximum allowable temperature of the FRP, and t_{FRP} is the dimensional thickness of the FRP layer. The non-dimensional temperature is measured for $t \in]0, 10]$ over two small areas located near the surface: Output 1, denoted by s^1 for the model and g^1 for the experimental measurement, is the average temperature over a small region around $x_1 = 0$; and Output 2, denoted by s^2 for the model and g^2 for the experimental measurement, is taken over a small region around $x_1 = 14.5$.

From the problem description it is evident that the temperature distribution, and hence the measured surface temperatures, g^1 and g^2 , depend on the (unknown) delamination width, w_{del} , and the (unknown) ratio of the conductivities, κ . By virtue of symmetry, we consider only the half-domain, and hence we take the half-width of the delamination, $H = w_{\text{del}}/2$, as our first (unknown) parameter μ^1 ; we take the thermal conductivity ratio, κ , as our second (unknown) parameter μ^2 . We assume that the delamination half-width satisfies $1 \leq H \leq 10$ and that the ratio of the conductivities satisfies $0.4 \leq \kappa \leq 1.8$; we thus obtain $(\mu \equiv (\mu^1, \mu^2) \equiv (H, \kappa) \in \mathcal{D} \equiv [1, 10] \times [0.4, 1.8] \subset \mathbf{R}^{P=2}$ as our parameter domain.

Appendix B provides the details of the exact governing equations in strong form,

the identification of the affine assumptions (9)-(11), and verification of our hypotheses of parametric coercivity (12)-(15). Additional details are provided in [11, 13].

We next introduce a temporal “truth approximation”: Euler backward discretization of the governing equations with timestep $\Delta t = 0.05$; this timestep is sufficiently small to capture the relevant dynamics for all values of the parameter $\mu \in \mathcal{D}$. Thus our time interval of $[0, 10]$ maps to discrete time levels $t^k = k\Delta t \forall k \in \mathbb{K} = \{1, \dots, K = 200\}$. Finally, we introduce a spatial \mathbb{P}^1 finite element truth approximation space Y of dimension $\mathcal{N}_t = 5603$ corresponding to a triangulation with very high resolution in the vicinity of the surface (which develops sharp gradients for small times) and in the region near the delamination crack; for our purposes here, this highly accurate “truth” approximation is indistinguishable from the exact solution.

In what follows, we present numerical results in Section 4.2 for our RB output bound method for the forward problem and in Section 4.3 for our parameter estimation procedure for the inverse problem.

4.2. RB Output Bounds

We first present the convergence rates and error bounds for the $I = 2$ outputs. For this purpose, we define the maximum relative output error $\epsilon_{\max, \text{rel}}^s$, the maximum relative output bound $\Delta_{\max, \text{rel}}^s$, and the average output effectivity $\bar{\eta}^s$ as:

$$\begin{aligned} \epsilon_{\max, \text{rel}}^s &= \max_{\mu \in \Xi_{\text{Test}}} |s(\mu, t_\eta(\mu)) - s_N(\mu, t_\eta(\mu))| / s_{\max} \\ \Delta_{\max, \text{rel}}^s &= \max_{\mu \in \Xi_{\text{Test}}} \Delta_N^s(\mu, t^K) / |s_{\max}| \\ \bar{\eta}^s &= \text{mean}_{\mu \in \Xi_{\text{Test}}} \Delta_N^s(\mu, t_\eta(\mu)) / |s(\mu, t_\eta(\mu)) - s_N(\mu, t_\eta(\mu))|; \end{aligned}$$

here $t_\eta(\mu) \equiv \arg \max_{t^k \in \mathbb{T}} |s(\mu, t^k) - s_N(\mu, t^k)|$, $s_{\max} \equiv \max_{t^k \in \mathbb{T}} \max_{\mu \in \Xi_{\text{Test}}} |s(\mu, t^k)|$, and $\Xi_{\text{Test}} \subset \mathcal{D}$ is an input sample of size 121 (a regular 11×11 grid). We present, as a function of $N_{\text{pr}} = N_{\text{du}}$, $\epsilon_{\max, \text{rel}}^s$, $\Delta_{\max, \text{rel}}^s$, and $\bar{\eta}^s$ in Table 1 for output 1 and Table 2 for output 2. We observe that the output error and output bound converge very rapidly: we need only $N_{\text{pr}} = N_{\text{du}} = 60$ to obtain an accuracy of approximately 0.22% in the output bound for output 1; even $N_{\text{pr}} = N_{\text{du}} = 40$ gives an accuracy of 0.36% in output

N_{pr}	N_{du}	$\epsilon_{\text{max,rel}}^s$	$\Delta_{\text{max,rel}}^s$	$\bar{\eta}^s$
20	20	1.78 E−02	1.23 E+00	174
40	40	1.75 E−03	3.85 E−02	260
60	60	1.67 E−04	2.24 E−03	189
80	80	7.57 E−06	2.43 E−04	268
100	100	6.21 E−07	3.21 E−05	222
120	120	1.34 E−07	6.84 E−06	212
140	140	3.36 E−08	1.82 E−06	210
160	160	8.64 E−09	4.14 E−07	384

Table 1. Convergence rates and effectivities for output 1.

N_{pr}	N_{du}	$\epsilon_{\text{max,rel}}^s$	$\Delta_{\text{max,rel}}^s$	$\bar{\eta}^s$
20	20	7.53 E−04	2.72 E−01	817
40	40	8.32 E−05	3.59 E−03	636
60	60	7.82 E−06	2.35 E−04	242
80	80	1.07 E−06	2.21 E−05	324
100	100	7.96 E−08	3.34 E−06	274
120	120	6.02 E−09	8.30 E−07	258

Table 2. Convergence rates and effectivities for output 2.

$N_{\text{pr}} = N_{\text{du}}$	$s_N(\mu, t^k), \forall k \in \mathbb{K}$	$\Delta_N^s(\mu, t^k), \forall k \in \mathbb{K}$	$s(\mu, t^k), \forall k \in \mathbb{K}$
20	3.11 E−03	9.78 E−04	1
40	5.22 E−03	1.54 E−03	1
60	7.90 E−03	2.34 E−03	1
80	9.49 E−03	3.88 E−03	1
100	1.48 E−02	9.98 E−03	1
120	2.01 E−02	1.74 E−02	1
140	2.55 E−02	3.21 E−02	1
160	3.10 E−02	4.36 E−02	1

Table 3. Online computational times to calculate $s_N(\mu, t^k)$ and $\Delta_N^s(\mu, t^k)$ for all $k \in \mathbb{K}$ (normalized with respect to the time to solve for $s(\mu, t^k), \forall k \in \mathbb{K}$) for output 1.

2. The error bound effectivities are quite large, $O(100)$, for all values of N_{pr} and N_{du} indicating that our bounds are not too sharp; however, thanks to the rapid convergence of the RB approximation, $O(100)$ effectivities do not significantly affect efficiency — the necessary increase in RB dimension N is typically modest.

Finally, we present in Table 3, as a function of $N_{\text{pr}} (= N_{\text{du}})$, the online computational

time to calculate $s_N(\mu, t^k)$ and $\Delta_N^s(\mu, t^k)$, $\forall k \in \mathbb{K}$, for output 1. The values are normalized with respect to the computational time for the direct calculation of the truth approximation output $s(\mu, t^k) = \ell(u(\mu, t^k))$, $\forall k \in \mathbb{K}$. We note that the time to compute $s_N(\mu, t^k)$ dominates the time to compute $\Delta_N^s(\mu, t^k)$ for small values of $N_{\text{pr}} = N_{\text{du}}$: this is due to the K^2 -complexity of evaluating the residual correction term. Since K is not too large in the present example we still obtain computational savings of a factor of 125 for $N_{\text{pr}} = N_{\text{du}} = 60$ (corresponding to an accuracy in the output bound of 0.22%); the average actual run-time for the output estimate and output bound in MATLAB 6.5 is 0.5 seconds on a 750 MHz Pentium III (all timings are for this hardware). The significant savings per output evaluation is crucial for many-query real-time performance in our parameter estimation procedure.

4.3. Parameter Estimation

In order to test our parameter estimation procedure, we choose a parameter value μ^* (unknown to the procedure, but known to us) and solve the forward problem for $s^i(\mu^*, t_j^{k_{\text{exp}}})$, $i = 1, 2$; then, for a given $\varepsilon_{\text{exp}} > 0$, we set the “synthetic” measurements as

$$G_{ij}^L = s^i(\mu^*, t_j^{k_{\text{exp}}}) - \varepsilon_{\text{exp}} s_{\text{max}}(\mu^*), \quad 1 \leq j \leq J, i \in \mathbb{S}, \quad (64)$$

$$G_{ij}^U = s^i(\mu^*, t_j^{k_{\text{exp}}}) + \varepsilon_{\text{exp}} s_{\text{max}}(\mu^*), \quad 1 \leq j \leq J, i \in \mathbb{S}, \quad (65)$$

with $s_{\text{max}}(\mu^*) = \max_{i \in \mathbb{S}} \max_{k \in \mathbb{K}_{\text{exp}}} s^i(\mu^*, t^k)$. Here \mathbb{S} is the set of indices indicating which outputs are invoked in the parameter estimation procedure; for instance, for $\mathbb{S} = \{1\}$ only s^1 is employed, whereas for $\mathbb{S} = \{1, 2\}$ both s^1 and s^2 are employed. Note that $s^i(\mu^*, t_j^{k_{\text{exp}}}) \in [G_{ij}^L, G_{ij}^U]$, $1 \leq i \leq I, 1 \leq j \leq J$; hence, the region \mathcal{P} as defined in (44) must contain μ^* , as must \mathcal{P}_N from Proposition 3.1 and \mathcal{R}_N from Proposition 3.2.

We begin by presenting a sample solution of the parameter estimation problem. We assume that the true parameter value is $\mu^* = (4, 1.2)$, that the measurement error is $\varepsilon_{\text{exp}} = 0.005$, that the set of measurement outputs is $\mathbb{S} = \{1, 2\}$, and that we are privy to measurements taken at $\mathbb{K}_{\text{exp}} = \{10, 20, \dots, 200\}$. We choose for the dimension of the RB approximations $N = 50$; recall that $N = N_{\text{pr}} = N_{\text{du}}$ indicates the dimension of both

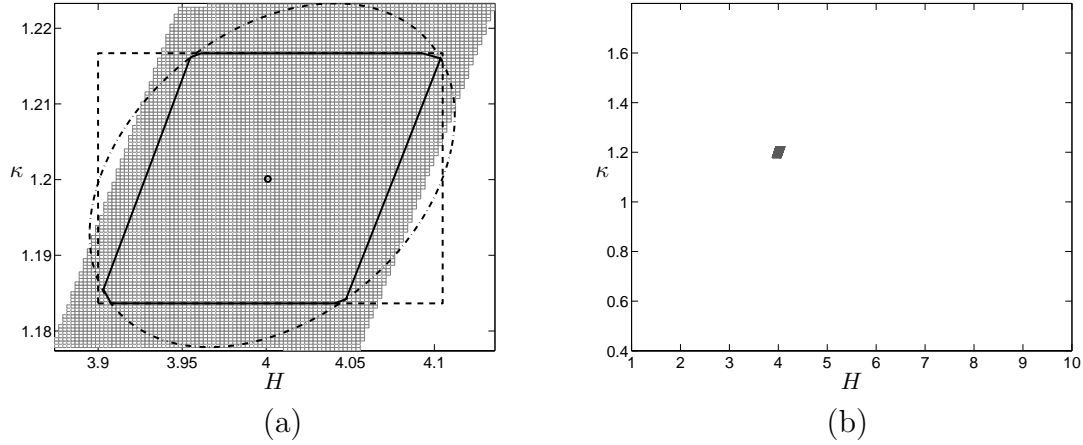


Figure 2. Sample solution of the parameter estimation problem: (a) μ_{IC} (open circle), $\tilde{\mathcal{P}}_N$ (solid line), $\tilde{\mathcal{E}}_N$ (dash-dot line), $\tilde{\mathcal{B}}_N$ (dashed line), and \mathcal{R}_N (the gray grid of cells) for $\varepsilon_{\text{exp}} = 0.005$ presented at “close-up” view; and (b) \mathcal{R}_N present at original view in the full parameter domain, \mathcal{D} . The true parameter is $(H^*, \kappa^*) = (4, 1.2)$.

the primal and dual RB approximations. The offline stage is then performed only once: it requires 18120 seconds or roughly 5 hours.

Given this problem specification, we solve the problem (47) to obtain $\mu_{IC} = (4.0009, 1.2001)$ in 5.6 seconds. (Henceforth all timings are for the online/deployed stage only.) We then find the boundary points $\{\hat{\mu}_1, \dots, \hat{\mu}_M\}$ for $M = 81$ search directions and construct $\tilde{\mathcal{P}}_N$ and $\tilde{\mathcal{E}}_N$ in a total of 1115 forward evaluations and 510.8 seconds. We next construct $\tilde{\mathcal{B}}_N$ in a total of 310 forward evaluations and 143.4 seconds. Finally, we form \mathcal{R}_N (for $L_{\text{ref}} = 12$) in a total of 7431 forward evaluations and 3404 seconds. (The region \mathcal{R}_N is constructed by starting with a grid of $M_0 = 1$ cell (the entire parameter domain) and refining the $\chi(m) = 1$ cells into 4 rectangular subcells for each iterative refinement.) We present the results in Figure 2; as we confirm further below, this inverse problem is identifiable. We note that \mathcal{R}_N is slightly larger than $\tilde{\mathcal{P}}_N$: our bounds for the output sensitivities, $\nabla s^i(\bar{\mu}_m, t^k)$, are rather large such that — at this level of refinement — $\nabla s^i(\bar{\mu}_m, t^k)\delta_m$ is greater than $\varepsilon_{\text{exp}} = 0.005$.

We next consider the sensitivity of the parameter estimation problem with respect to the measurement error ε_{exp} and the number of refinements L_{ref} . For this purpose, we introduce $\widetilde{\Delta H} = \max_{\mathcal{R}_N} H - \min_{\mathcal{R}_N} H$. We present in Figure 3(a) $\widetilde{\Delta H}$ as a function

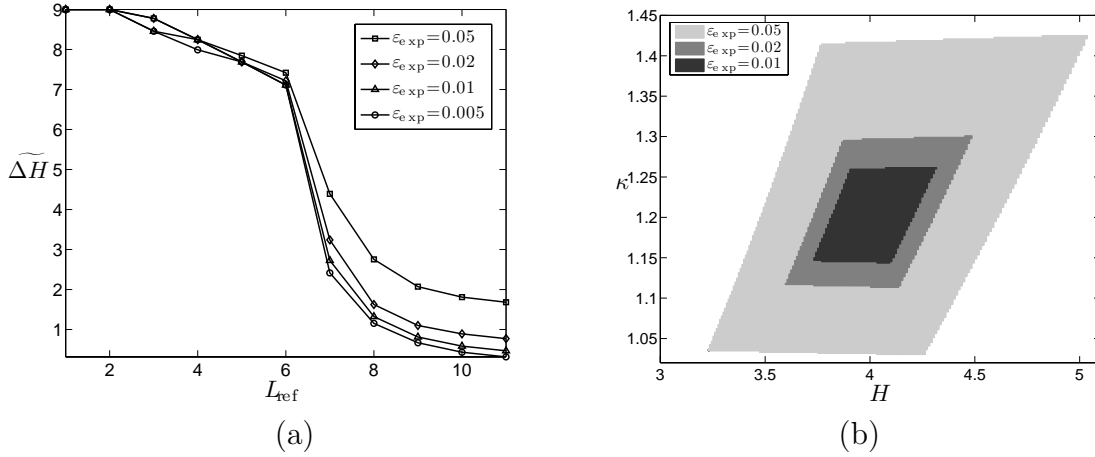


Figure 3. Effect of the measurement error and the number of refinements on \mathcal{R}_N : (a) $\widetilde{\Delta H}$ as a function of ε_{exp} and L_{ref} , and (b) \mathcal{R}_N as a function of ε_{exp} for $L_{\text{ref}} = 10$. The true parameter is $(H^*, \kappa^*) = (4, 1.2)$.

of ε_{exp} and L_{ref} for $(H^*, \kappa^*) = (4, 1.2)$; as before, $N = 50$, $\mathbb{K}_{\text{exp}} = \{10, 20, \dots, 200\}$, and $\mathbb{S} = \{1, 2\}$. The “estimation accuracy” $\widetilde{\Delta H}$ falls sharply at $L_{\text{ref}} = 6$ and then decreases gradually for $L_{\text{ref}} > 6$: increasing the number of refinements effectively reduces the uncertainty in the parameter estimate, albeit at higher computational costs; however, there is an optimal value of L_{ref} for a given ε_{exp} beyond which the achievable improvement is very small. (Similar results and conclusions apply to refinement of the RB approximation as measured by N .) Furthermore, as shown in Figure 3(b) for $L_{\text{ref}} = 10$, \mathcal{R}_N shrinks toward the true parameter value $(H^*, \kappa^*) = (4, 1.2)$ as ε_{exp} decreases, indicative of an identifiable problem.

We next study the sensitivity with respect to the specific outputs measured and the number of outputs measured. We assume that the true parameter is $(H^*, \kappa^*) = (7.5, 1.4)$, that the measurement error is $\varepsilon_{\text{exp}} = 0.005$, and that measurements are taken at $\mathbb{K}_{\text{exp}} = \{10, 20, \dots, 200\}$; as before we choose $N = 50$. We present in Figure 4 the three bounding ellipses for $\mathbb{S}_1 = \{2\}$, $\mathbb{S}_2 = \{1\}$, and $\mathbb{S}_3 = \{1, 2\}$. We note that employing only the second output (on top of the undamaged region) results in a very poor estimate of the delamination half-width. Employing only the first output, on the other hand, results in a very good estimate of the delamination half-width. The result for $\mathbb{S}_3 = \{1, 2\}$ is only slightly better than the result for $\mathbb{S}_2 = \{1\}$ as regards the

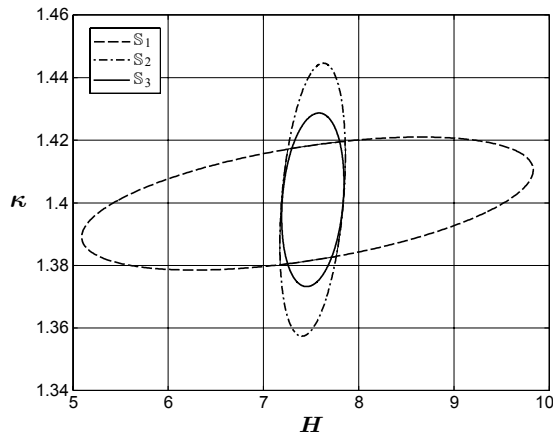


Figure 4. Effect of the specific outputs measured and the number of outputs measured: $\tilde{\mathcal{E}}_N$ for $\mathbb{S}_1 = \{2\}$, $\mathbb{S}_2 = \{1\}$, and $\mathbb{S}_3 = \{1, 2\}$. The true parameter is $(H^*, \kappa^*) = (7.5, 1.4)$.

uncertainty in H .

We further investigate the sensitivity of the parameter estimation but now with respect to the number of measurements in time. We assume that $(H^*, \kappa^*) = (7.5, 1.4)$, $\varepsilon_{\text{exp}} = 0.005$, and $N = 50$. We consider two different time-discrete sets: $\mathbb{K}_{\text{exp}}^1 \equiv \{10, 20, \dots, 100\}$ and $\mathbb{K}_{\text{exp}}^2 \equiv \{10, 20, \dots, 200\}$. We plot the bounding ellipses for these two cases in Figure 5. We observe that the longer observation time considerably decreases the uncertainty in the (important) H^* estimate, but has no effect on reducing the uncertainty in the (relatively unimportant) κ^* estimate. Since the size of \mathbb{K}_{exp} strongly affects the computational efficiency, the choice of \mathbb{K}_{exp} should reflect the trade-off between acceptable uncertainty and acceptable response time.

Finally, we apply the procedure to a problem which is non-identifiable (ill-posed) due to insufficient measurements. For this purpose, we consider $(H^*, \kappa^*) = (6.0, 1.0)$ and only *one* measurement, $\mathbb{K}_{\text{exp}}^3 \equiv \{100\}$, for a single output, $\mathbb{S} = \{2\}$. Here we take $N = 100$ to ensure that the RB error is smaller than the measurement error. We show $\tilde{\mathcal{E}}_N$ in Figure 6 for very small measurement errors of 0.02% and 0.01%. Because we use only one measurement to predict two parameters, the bounds on the H^* estimate are considerably larger than the measurement error: for $\varepsilon_{\text{exp}} = 0.0001$ (0.01%), the uncertainty in the H^* estimate is approximately 65%, meaning that the noise is amplified

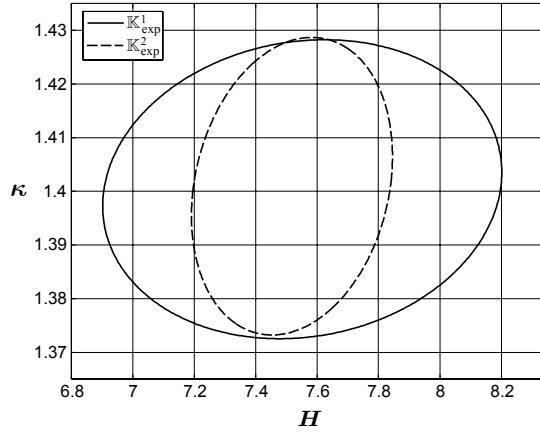


Figure 5. Effect of the measurements in time: $\tilde{\mathcal{E}}_N$ for $\mathbb{K}_{\text{exp}}^1 \equiv \{10, 20, \dots, 100\}$ and $\mathbb{K}_{\text{exp}}^2 \equiv \{10, 20, \dots, 200\}$. The true parameter is $(H^*, \kappa^*) = (7.5, 1.4)$.

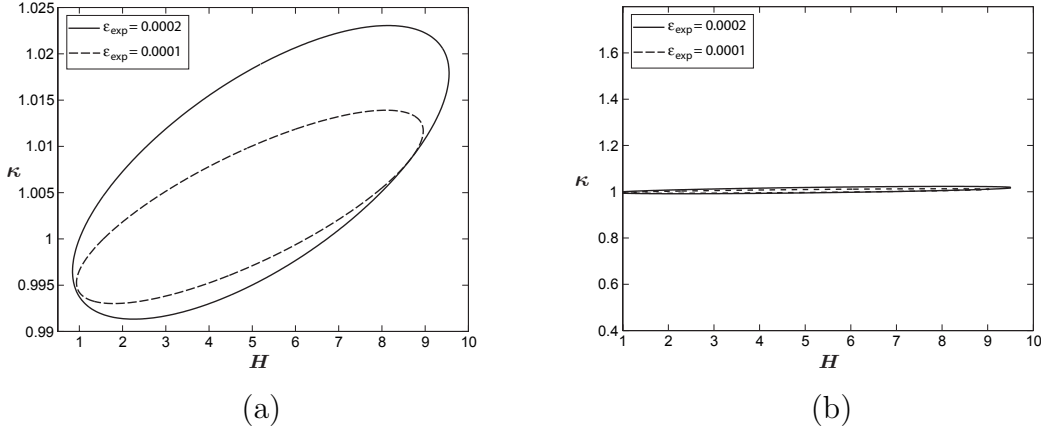


Figure 6. Verification of non-identifiability: $\tilde{\mathcal{E}}_N$ for the measurement errors of 0.0002 and 0.0001 for $\mathbb{K}_{\text{exp}}^3 \equiv \{100\}$ presented in (a) zoom view, and (b) original view in \mathcal{D} .

by a factor of 6500. Refinement of N , L_{ref} , or ε_{exp} will have little effect: fundamentally, the set \mathcal{P} is no longer a singleton and \mathcal{P} is of considerable extent in H .

Although we present our results here to illustrate the methodology, in actual practice we can apply the same calculations to either aid in the design of an effective Non-Destructive Evaluation procedure, or to perform parameter estimation in the field.

Acknowledgments

We would like to thank Professor Yvon Maday of University Paris VI and Dr. Karen Veroy of MIT for helpful discussions. This work was supported by DARPA and AFOSR under Grant FA9550-05-1-0114 and by the Singapore-MIT Alliance.

Appendix A. Bounds for the solution sensitivities

Lemma A.1. *Under the assumptions stated in Section 2.1, we have*

$$\sum_{j=1}^k m(y(\mu, t^j) - y(\mu, t^{j-1}), y(\mu, t^j) - y(\mu, t^{j-1}); \mu) \leq \frac{\Delta t}{\alpha(\mu)} \|b(\cdot; \mu)\|_{Y'}^2, \quad \forall k \in \mathbb{K}. \quad (\text{A.1})$$

Proof. We first introduce $z(\mu) \in Y$ (note $b \in Y'$) such that

$$a(z(\mu), v; \mu) = b(v; \mu), \quad \forall v \in Y, \quad (\text{A.2})$$

which then implies

$$a(z(\mu), z(\mu); \mu) = b(z(\mu); \mu) \leq \|b(\cdot; \mu)\|_{Y'} \|z(\mu)\|_Y \leq \frac{\|b(\cdot; \mu)\|_{Y'}^2}{\alpha(\mu)}. \quad (\text{A.3})$$

We further introduce an associated symmetric positive-definite eigenproblem: find $(\chi_i(\mu), \lambda_i(\mu)) \in Y \times \mathbb{R}$, $1 \leq i \leq \mathcal{N}$, such that

$$a(\chi_i(\mu), v; \mu) = \lambda_i(\mu) m(\chi_i(\mu), v; \mu), \quad m(\chi_i(\mu), \chi_i(\mu)) = 1. \quad (\text{A.4})$$

We order the eigenvalues such that $0 < \lambda_{\min}(\mu) = \lambda_1(\mu) \leq \dots \leq \lambda_{\mathcal{N}}(\mu)$. We note the orthogonality relation $a(\chi_i(\mu), \chi_j(\mu)) = \lambda_i(\mu) m(\chi_i(\mu), \chi_j(\mu)) = \lambda_i(\mu) \delta_{ij}$, $1 \leq i, j \leq \mathcal{N}$.

We now expand $y(\mu, t^k) = \sum_{i=1}^{\mathcal{N}} \phi_i^k(\mu) \chi_i(\mu)$, $1 \leq k \leq K$, as well as $z(\mu) = \sum_{i=1}^{\mathcal{N}} z_i(\mu) \chi_i(\mu)$; note from (A.2) that $z_i(\mu) = b(\chi_i(\mu); \mu) / \lambda_i(\mu)$. We substitute these expansions into (3) and invoke orthogonality to obtain

$$\frac{\phi_i^k(\mu) - \phi_i^{k-1}(\mu)}{\Delta t} + \lambda_i(\mu) \phi_i^k(\mu) = \lambda_i(\mu) z_i(\mu), \quad 1 \leq i \leq \mathcal{N}, 1 \leq k \leq K, \quad (\text{A.5})$$

with $\phi_i^0(\mu) = 0$, $1 \leq i \leq \mathcal{N}$. This yields

$$\phi_i^k(\mu) = \frac{\lambda_i \Delta t z_i(\mu) + \phi_i^{k-1}(\mu)}{1 + \lambda_i(\mu) \Delta t} = z_i(\mu) f^k(\lambda_i(\mu) \Delta t), \quad 1 \leq i \leq \mathcal{N}, 1 \leq k \leq K, \quad (\text{A.6})$$

where

$$f^1(x) = \frac{x}{1+x}, \quad f^2(x) = \frac{x + f^1(x)}{1+x}, \dots, f^k(x) = \frac{x + f^{k-1}(x)}{1+x}; \quad (\text{A.7})$$

we note that

$$\sum_{j=1}^k (1 - f^j(x))^2 = \sum_{j=1}^k \frac{1}{(1+x)^{2j}} = \frac{(1+x)^{2k} - 1}{(x^2 + 2x)(1+x)^{2k}} \leq \frac{1}{x}, \quad \forall x > 0. \quad (\text{A.8})$$

It thus follows from (A.3)-(A.8) and the orthogonality that

$$\begin{aligned}
\sum_{j=1}^k m(y(t^j) - y(t^{j-1}), y(t^j) - y(t^{j-1}); \mu) &= \sum_{j=1}^k \sum_{i=1}^{\mathcal{N}} (\phi_i^j(\mu) - \phi_i^{j-1}(\mu))^2 \\
&= \sum_{j=1}^k \sum_{i=1}^{\mathcal{N}} (\Delta t)^2 \lambda_i^2(\mu) (z_i(\mu) - \phi_i^j(\mu))^2 \\
&= (\Delta t)^2 \sum_{i=1}^{\mathcal{N}} \lambda_i^2(\mu) z_i^2(\mu) \sum_{j=1}^k (1 - f^j(\lambda_i(\mu) \Delta t))^2 \\
&\leq \Delta t \sum_{i=1}^{\mathcal{N}} \lambda_i(\mu) z_i^2(\mu) \\
&\leq \Delta t a(z(\mu), z(\mu); \mu) \\
&\leq \frac{\Delta t}{\alpha(\mu)} \|b(\cdot; \mu)\|_{Y'}^2, \tag{A.9}
\end{aligned}$$

which is the desired result. \square

Lemma A.2. *Under the assumptions stated in Section 2.1, we have*

$$\Delta t \sum_{j=1}^k a(y(\mu, t^j), y(\mu, t^j); \mu) \leq \frac{k \Delta t}{\alpha(\mu)} \|b(\cdot; \mu)\|_{Y'}^2. \tag{A.10}$$

Proof. We choose $v = y(t^j)$ in (3) to obtain

$$\begin{aligned}
m(y(t^j), y(t^j); \mu) + \Delta t a(y(t^j), y(t^j); \mu) &= m(y(t^{j-1}), y(t^j); \mu) \\
+ \Delta t b(y(t^j); \mu), \quad \forall v \in Y, \forall j \in \mathbb{K}. \tag{A.11}
\end{aligned}$$

We next note from the Cauchy-Schwartz and Young inequalities that

$$\begin{aligned}
m(y(t^{j-1}), y(t^j); \mu) &\leq m^{1/2}(y(t^{j-1}), y(t^{j-1}); \mu) m^{1/2}(y(t^j), y(t^j); \mu) \\
&\leq \frac{1}{2} m(y(t^{j-1}), y(t^{j-1}); \mu) + \frac{1}{2} m(y(t^j), y(t^j); \mu). \tag{A.12}
\end{aligned}$$

It thus follows from (A.11) and (A.12) that

$$m(y(t^j), y(t^j); \mu) - m(y(t^{j-1}), y(t^{j-1}); \mu) + 2\Delta t a(y(t^j), y(t^j); \mu) \leq 2\Delta t b(y(t^j); \mu)$$

which after performing the sum from $j = 1$ to k gives

$$m(y(t^k), y(t^k); \mu) + 2\Delta t \sum_{j=1}^k a(y(t^j), y(t^j); \mu) = 2\Delta t \sum_{j=1}^k b(y(t^j); \mu). \tag{A.13}$$

Furthermore, we apply the Cauchy-Schwartz inequality and coercivity to bound the right-hand side as

$$2\Delta t \sum_{j=1}^k b(y(t^j); \mu) \leq 2\Delta t \sum_{j=1}^k \|b(\cdot; \mu)\|_{Y'} \|y(t^j)\|_Y$$

$$\begin{aligned}
&\leq 2\Delta t \{k\|b(\cdot; \mu)\|_{Y'}^2\}^{1/2} \left\{ \sum_{j=1}^k \|y(t^j)\|_Y^2 \right\}^{1/2} \\
&\leq 2\Delta t \{k\|b(\cdot; \mu)\|_{Y'}^2\}^{1/2} \left\{ \frac{1}{\alpha(\mu)} \sum_{j=1}^k a(y(t^j), y(t^j); \mu) \right\}^{1/2}. \quad (\text{A.14})
\end{aligned}$$

The desired result follows from (A.13) and (A.14). \square

Proposition A.3. *Under the assumptions stated in Section 2.1 and Section 3.3, the sensitivities for the solution are bounded as*

$$m\left(\frac{\partial y(t^k)}{\partial \mu^p}, \frac{\partial y(t^k)}{\partial \mu^p}; \mu\right) \leq 2k\Delta t \left(\frac{2\Upsilon_m^p(\mu) + \Upsilon_a^p(\mu)}{\alpha(\mu)} \right) \|b(\cdot; \mu)\|_{Y'}^2 + \frac{2k\Delta t}{\alpha(\mu)} \left\| \frac{\partial b(\cdot; \mu)}{\partial \mu^p} \right\|_{Y'}^2. \quad (\text{A.15})$$

Proof. Let the prime denote the partial derivatives with respect to a particular parameter component μ^p . We first differentiate (3) with respect to μ^p and choose $v = y'(\mu, t^j)$ to obtain

$$\begin{aligned}
&m(y'(t^j), y'(t^j); \mu) + m'(y(t^j), y'(t^j); \mu) + \Delta t a(y'(t^j), y'(t^j); \mu) + \Delta t a'(y(t^j), y'(t^j); \mu) \\
&\quad = m(y'(t^{j-1}), y'(t^j); \mu) + m'(y(t^{j-1}), y'(t^j); \mu) + \Delta t b'(y'(t^j); \mu). \quad (\text{A.16})
\end{aligned}$$

We then note from the Cauchy-Schwartz and Young inequalities that

$$\begin{aligned}
&m(y'(t^{j-1}), y'(t^j); \mu) \leq m^{1/2}(y'(t^{j-1}), y'(t^{j-1}); \mu) m^{1/2}(y'(t^j), y'(t^j); \mu) \\
&\quad \leq \frac{1}{2}m(y'(t^{j-1}), y'(t^{j-1}); \mu) + \frac{1}{2}m(y'(t^j), y'(t^j); \mu). \quad (\text{A.17})
\end{aligned}$$

It thus follows from (A.16) and (A.17) that

$$\begin{aligned}
&m(y'(t^j), y'(t^j); \mu) - m(y'(t^{j-1}), y'(t^{j-1}); \mu) + 2\Delta t a(y'(t^j), y'(t^j); \mu) \\
&\quad \leq 2(m'(y(t^{j-1}), y'(t^j); \mu) - m'(y(t^j), y'(t^j); \mu)) \\
&\quad \quad - 2\Delta t a'(y(t^j), y'(t^j); \mu) + 2\Delta t b'(y'(t^j); \mu), \quad (\text{A.18})
\end{aligned}$$

which, after performing the sum from $j = 1$ to k , gives

$$\begin{aligned}
&m(y'(t^k), y'(t^k); \mu) + 2\Delta t \sum_{j=1}^k a(y'(t^j), y'(t^j); \mu) \\
&\quad \leq 2 \sum_{j=1}^k (m'(y(t^{j-1}), y'(t^j); \mu) - m'(y(t^j), y'(t^j); \mu)) \\
&\quad \quad - 2\Delta t \sum_{j=1}^k a'(y(t^j), y'(t^j); \mu) + 2\Delta t \sum_{j=1}^k b'(y'(t^j); \mu). \quad (\text{A.19})
\end{aligned}$$

We proceed to obtain bounds for the terms on the right-hand side.

The first term in the right hand side can be bounded by

$$\begin{aligned}
& 2 \sum_{j=1}^k m'(y(t^{j-1}) - y(t^j), y'(t^j); \mu) \\
&= 2 \sum_{j=1}^k \sum_{q=1}^{Q_m} (\Theta_m^q(\mu))' m^q(y(t^{j-1}) - y(t^j), y'(t^j)) \\
&\leq 2 \sum_{j=1}^k \sum_{q=1}^{Q_m} |(\Theta_m^q(\mu))'| \sqrt{m^q(y(t^{j-1}) - y(t^j), y(t^{j-1}) - y(t^j))} \sqrt{m^q(y'(t^j), y'(t^j))} \\
&\leq \sum_{j=1}^k \sum_{q=1}^{Q_m} |(\Theta_m^q(\mu))'| \left(\frac{2k |(\Theta_m^q(\mu))'|}{\Theta_m^q(\mu)} m^q(y(t^{j-1}) - y(t^j), y(t^{j-1}) - y(t^j)) \right. \\
&\quad \left. + \frac{\Theta_m^q(\mu)}{2k |(\Theta_m^q(\mu))'|} m^q(y'(t^j), y'(t^j)) \right) \\
&\leq 2k \Upsilon_m^p(\mu) \sum_{j=1}^k m(y(t^{j-1}) - y(t^j), y(t^{j-1}) - y(t^j); \mu) + \frac{1}{2k} \sum_{j=1}^k m(y'(t^j), y'(t^j); \mu) \tag{A.20}
\end{aligned}$$

where we have applied the Cauchy-Schwartz inequality in the third step, and the Young inequality

$$2|c||d| \leq \frac{c^2}{\rho^2} + \rho^2 d^2 \tag{A.21}$$

for $c^2 = m^q(y(t^{j-1}) - y(t^j), y(t^{j-1}) - y(t^j))$, $d^2 = m^q(y'(t^j), y'(t^j))$, and $\rho^2 = \frac{\Theta_m^q(\mu)}{2k |(\Theta_m^q(\mu))'|}$ in the fourth step; note our derivation remains valid for $(\Theta_m^q(\mu))' = 0$ since in this case the associated term vanishes.

In a similar way, we can bound the second term on the right-hand side of the equation (A.19) as

$$-2\Delta t \sum_{j=1}^k a'(y(t^j), y'(t^j); \mu) \leq \Delta t \sum_{j=1}^k (\Upsilon_a^p(\mu) a(y(t^j), y'(t^j); \mu) + a(y'(t^j), y'(t^j); \mu)). \tag{A.22}$$

We can also develop a bound for the last term from Cauchy-Schwartz inequality and coercivity:

$$\begin{aligned}
2\Delta t \sum_{j=1}^k b'(y'(t^j); \mu) &\leq 2\Delta t \sum_{j=1}^k \|b'(\cdot; \mu)\|_{Y'} \|y'(t^j)\|_Y \\
&\leq 2\Delta t \{k \|b'(\cdot; \mu)\|_{Y'}^2\}^{1/2} \left\{ \sum_{j=1}^k \|y'(t^j)\|_Y^2 \right\}^{1/2}
\end{aligned}$$

$$\begin{aligned}
&\leq 2\Delta t \{k\|b(\cdot; \mu)\|_{Y'}^2\}^{1/2} \left\{ \frac{1}{\alpha(\mu)} \sum_{j=1}^k a(y'(t^j), y'(t^j); \mu) \right\}^{1/2} \\
&\leq \frac{k\Delta t}{\alpha(\mu)} \|b'(\cdot; \mu)\|_{Y'}^2 + \Delta t \sum_{j=1}^k a(y'(t^j); y'(t^j); \mu). \tag{A.23}
\end{aligned}$$

Gathering (A.19), (A.20), (A.22), and (A.23) gives

$$\begin{aligned}
&m(y'(t^k), y'(t^k); \mu) - \frac{1}{2k} \sum_{j=1}^k m(y'(t^j), y'(t^j); \mu) \\
&\leq 2k\Upsilon_m^p(\mu) \sum_{j=1}^k m(y(t^{j-1}) - y(t^j), y(t^{j-1}) - y(t^j); \mu) \\
&\quad + \Upsilon_a^p(\mu) \Delta t \sum_{j=1}^k a(y(t^j), y(t^j); \mu) + \frac{k\Delta t}{\alpha(\mu)} \|b'(\cdot; \mu)\|_{Y'}^2, \\
&\leq k\Delta t \left(\frac{2\Upsilon_m^p(\mu) + \Upsilon_a^p(\mu)}{\alpha(\mu)} \right) \|b(\cdot; \mu)\|_{Y'}^2 + \frac{k\Delta t}{\alpha(\mu)} \|b'(\cdot; \mu)\|_{Y'}^2, \tag{A.24}
\end{aligned}$$

according to Lemma A.1 and Lemma A.2.

Finally, we proceed by induction to get the desired result. The result is obvious for $k = 1$. Assuming that the result is true for $j < k$, we proceed by induction. For any k for which $m(y'(t^k), y'(t^k); \mu)$ is the maximum, the result is again obvious. For any k for which $m(y'(t^j), y'(t^j); \mu)$ is the maximum for some $j < k$, our induction hypothesis yields

$$\begin{aligned}
&m(y'(t^k), y'(t^k); \mu) \leq m(y'(t^j), y'(t^j); \mu) \\
&\leq 2j\Delta t \left(\frac{2\Upsilon_m^p(\mu) + \Upsilon_a^p(\mu)}{\alpha(\mu)} \right) \|b(\cdot; \mu)\|_{Y'}^2 + \frac{2j\Delta t}{\alpha(\mu)} \|b'(\cdot; \mu)\|_{Y'}^2, \\
&\leq 2k\Delta t \left(\frac{2\Upsilon_m^p(\mu) + \Upsilon_a^p(\mu)}{\alpha(\mu)} \right) \|b(\cdot; \mu)\|_{Y'}^2 + \frac{2k\Delta t}{\alpha(\mu)} \|b'(\cdot; \mu)\|_{Y'}^2, \tag{A.25}
\end{aligned}$$

which is the desired result. \square

Appendix B. Concrete Delamination

Appendix B.1. Governing Equations

The temperature distribution, $T(x, t)$, in the FRP and concrete (C) is governed by the (appropriately) non-dimensionalized *transient* heat equations

$$\frac{\partial T_{\text{FRP}}(x, t)}{\partial t} = \kappa \nabla^2 T_{\text{FRP}}(x, t), \quad \text{in } \Omega_{\text{FRP}}^o, \tag{B.1}$$

$$\frac{\partial T_C(x, t)}{\partial t} = \nabla^2 T_C(x, t), \quad \text{in } \Omega_C^o, \quad (\text{B.2})$$

with initial temperatures $T_{\text{FRP}}(x, t = 0) = 0$ and $T_C(x, t = 0) = 0$; here, $x = (x_1, x_2)$ is the spatial coordinate, and $T(x, t) = (\bar{T} - \bar{T}_0)/(\bar{T}_{\text{FRP, max}} - \bar{T}_0)$ is the non-dimensional temperature, where \bar{T}_0 is the ambient temperature and $\bar{T}_{\text{FRP, max}}$ is the maximum allowable temperature of the FRP.

The temperature and heat flux at the composite-concrete interface (excluding the delaminated area) are continuous, i.e.,

$$T_{\text{FRP}} = T_C, \quad \text{on } \partial\Omega_{\text{FRP}} \cap \partial\Omega_C, \quad (\text{B.3})$$

$$-\kappa \nabla T_{\text{FRP}} \cdot \mathbf{n}|_{\partial\Omega_{\text{FRP}}} = -\nabla T_C \cdot \mathbf{n}|_{\partial\Omega_C}, \quad \text{on } \partial\Omega_{\text{FRP}} \cap \partial\Omega_C. \quad (\text{B.4})$$

Since the conductivity of air is much larger than that of FRP and concrete, we may impose a homogeneous Neumann condition at the delamination boundary, Γ_{del} ,

$$\nabla T_{\text{FRP}} \cdot \mathbf{n} = 0, \quad \text{on } \Gamma_{\text{del}}, \quad (\text{B.5})$$

$$\nabla T_C \cdot \mathbf{n} = 0, \quad \text{on } \Gamma_{\text{del}}. \quad (\text{B.6})$$

The non-dimensional heat source $q(t)$ is reflected in the boundary condition on the surface, given by

$$-\kappa \nabla T_{\text{FRP}} \cdot \mathbf{n} = q(t), \quad \text{on } x_2 = 11, \quad x_1 \in [-30, 30], \quad (\text{B.7})$$

where $q(t) = 1$ for $t \in [0, 0.5]$ and $q(t) = 0$ for $t > 0.5$. Finally, we assume that the heat flux on the left and right boundaries is zero,

$$\nabla T_C \cdot \mathbf{n} = 0, \quad \text{on } x_1 = \pm 30, \quad x_2 \in [1, 10], \quad (\text{B.8})$$

$$\nabla T_{\text{FRP}} \cdot \mathbf{n} = 0, \quad \text{on } x_1 = \pm 30, \quad x_2 \in [10, 11], \quad (\text{B.9})$$

and that the temperature at the bottom boundary is at ambient level,

$$T_C = 0, \quad \text{on } x_1 \in [-30, 30], \quad x_2 = 0. \quad (\text{B.10})$$

Note that the dimensions of the domain are chosen such that the truncation boundary conditions (B.8)–(B.10) do not substantially affect the temperature measurements.

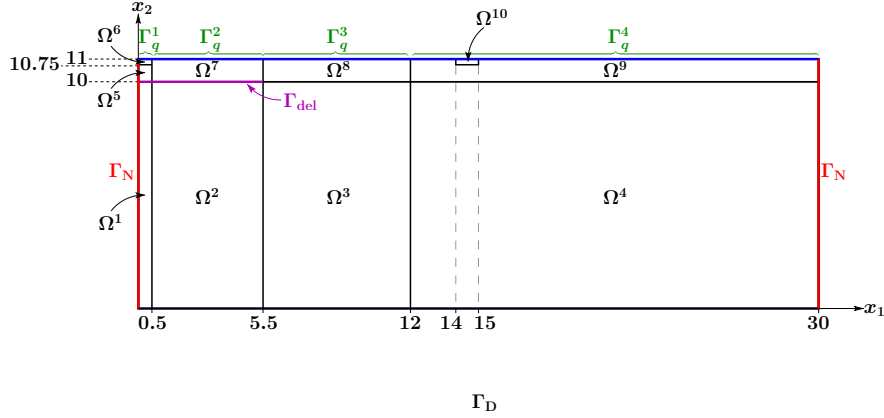


Figure B1. Reference domain $\Omega \equiv \Omega^o$ for $\mu_{1,\text{ref}} = 5$.

Appendix B.2. Mapped Reference Domain

We note that the geometry of the slab depends on the delamination width w_{del} ; we treat the geometric variation in an indirect way by performing an affine geometric mapping (see [33] for a detailed discussion of affine mappings) from the parameter dependent solution domain Ω^o (with solution T) to a fixed reference domain $\Omega \equiv \Omega^o = [0, 30] \times [0, 11]$ for $\mu_{1,\text{ref}} = 5$ (with solution y) shown in Figure B1.

As regards the transformation, we first divide Ω into 10 subdomains, Ω^i , $1 \leq i \leq 10$. The delamination is indicated by the magenta horizontal line, Γ_{del} , between the domains Ω^1 , Ω^2 and Ω^5 , Ω^7 , respectively. We note that we only have to consider geometric variations — dilation in the x_1 -direction — in regions Ω^2 , Ω^3 , Ω^7 , and Ω^8 ; the remaining regions do not vary with the delamination width w_{del} . We also note that the “fictitious” regions Ω_6 and Ω_{10} are introduced primarily to preserve the integrity of the two outputs — defined as the average temperatures over these regions.

Appendix B.3. Affine Decomposition

We define the inner product $(w, v)_Y \equiv a(w, v; \mu_{\text{ref}})$ and $(w, v)_X \equiv m(w, v; \mu_{\text{ref}})$, corresponding to (32) and (33) for $\mu_{\text{ref}} = (5, 1.2)$, respectively; the coercivity lower bounds $\alpha(\mu)$ and $\sigma(\mu)$ are then constructed by the “min Θ ” approach [23, 13].

It can be shown that in the reference domain the bilinear and linear forms a , m , and b admit the affine representation (9)-(11) with $Q_a = 10$, $Q_m = 3$, $Q_b = 3$, respectively.

The affine decomposition resulting from the geometric mapping is given as follows (note that the output functional, ℓ , does not depend on μ) [11, 13]:

$$\begin{aligned}
\Theta_a^1(\mu) &= 1 & a^1(w, v) &= \int_{\Omega^1 \cup \Omega^4} \nabla w \cdot \nabla v \\
\Theta_a^2(\mu) &= \mu_2 & a^2(w, v) &= \int_{\Omega^5 \cup \Omega^6 \cup \Omega^9 \cup \Omega^{10}} \nabla w \cdot \nabla v \\
\Theta_a^3(\mu) &= \frac{5}{\mu_1 - 0.5} & a^3(w, v) &= \int_{\Omega^2} w_x v_x \\
\Theta_a^4(\mu) &= \frac{\mu_1 - 0.5}{5} & a^4(w, v) &= \int_{\Omega^2} w_y v_y \\
\Theta_a^5(\mu) &= \frac{6.5}{12 - \mu_1} & a^5(w, v) &= \int_{\Omega^3} w_x v_x \\
\Theta_a^6(\mu) &= \frac{12 - \mu_1}{6.5} & a^6(w, v) &= \int_{\Omega^3} w_y v_y \\
\Theta_a^7(\mu) &= \mu_2 \frac{5}{\mu_1 - 0.5} & a^7(w, v) &= \int_{\Omega^7} w_x v_x \\
\Theta_a^8(\mu) &= \mu_2 \frac{\mu_1 - 0.5}{5} & a^8(w, v) &= \int_{\Omega^7} w_y v_y \\
\Theta_a^9(\mu) &= \mu_2 \frac{6.5}{12 - \mu_1} & a^9(w, v) &= \int_{\Omega^8} w_x v_x \\
\Theta_a^{10}(\mu) &= \mu_2 \frac{12 - \mu_1}{6.5} & a^{10}(w, v) &= \int_{\Omega^8} w_y v_y,
\end{aligned} \tag{B.11}$$

for $a(\cdot, \cdot; \mu)$;

$$\begin{aligned}
\Theta_m^1(\mu) &= 1 & m^1(w, v) &= \int_{\Omega^1 \cup \Omega^4 \cup \Omega^5 \cup \Omega^6 \cup \Omega^9 \cup \Omega^{10}} w v \\
\Theta_m^2(\mu) &= \frac{\mu_1 - 0.5}{5} & m^2(w, v) &= \int_{\Omega^2 \cup \Omega^7} w v \\
\Theta_m^3(\mu) &= \frac{12 - \mu_1}{6.5} & m^3(w, v) &= \int_{\Omega^3 \cup \Omega^8} w v,
\end{aligned} \tag{B.12}$$

for $m(\cdot, \cdot; \mu)$; and

$$\begin{aligned}
\Theta_b^1(\mu) &= 1 & b^1(w, v) &= \int_{\Gamma_1^1 \cup \Gamma_q^4} v d\Gamma \\
\Theta_b^2(\mu) &= \frac{\mu_1 - 0.5}{5} & b^2(w, v) &= \int_{\Gamma_q^2} v d\Gamma \\
\Theta_b^3(\mu) &= \frac{12 - \mu_1}{6.5} & b^3(w, v) &= \int_{\Gamma_q^3} v d\Gamma,
\end{aligned} \tag{B.13}$$

for $b(\cdot; \mu)$. (Note the superscripts for the Θ , a , m and b refer to the terms in the affine expansions not the subdomains.)

It is readily demonstrated that a and m are parametrically coercive.

References

- [1] O. M. Alifanov, E. A. Artyukhin, and I. Yu. Gejadze. Sequential regularized solution of one inverse heat conduction problem. *Soviet Mathematics Doklady*, 364(5):1–5, 1999.
- [2] O. M. Alifanov, E. A. Artyukhin, and S. V. Rumyantsev. *Extreme methods for solving ill-posed problems with applications to inverse problems*. New York: Begell House, 1995.
- [3] O. M. Alifanov and I. Yu. Gejadze. Thermal loads identification technique for materials and structures in real time. *Acta Astronautica*, 41(4):225–265, 1997.
- [4] E. Balmes. Parametric families of reduced finite element models: Theory and applications. *Mechanical Systems and Signal Processing*, 10(4):381–394, 1996.
- [5] H. T. Banks and K. Kunisch. *Estimation Techniques for Distributed Parameter Systems*. Birkhauser, Boston, 1989.
- [6] M. Barrault, Y. Maday, N. C. Nguyen, and A. T. Patera. An “empirical interpolation” method: Application to efficient reduced-basis discretization of partial differential equations. *C. R. Acad. Sci. Paris, Série I*, 339:667–672, 2004.
- [7] A. Baussard, Denis Prémel, and O. Venard. A bayesian approach for solving inverse scattering from microwave laboratory-controlled data. *Inverse Problems*, 17:1659–1669, 2001.
- [8] R. Becker and R. Rannacher. Weighted *a posteriori* error control in finite element methods. Technical report, Universität Heidelberg, 1996.
- [9] H. W. Engl, M. Hanke, and A. Neubauer. *Regularization of Inverse Problems*. Kluwer Academic, Dordrecht, 1996.
- [10] B. G. Fitzpatrick. Bayesian analysis in inverse problems. *Inverse Problems*, 7:675–702, 1991.
- [11] M. Grepl. *Reduced-Basis Approximations for Time-Dependent Partial Differential Equations: Application to Optimal Control*. PhD thesis, Massachusetts Institute of Technology, Cambridge, MA, May 2005.
- [12] M. A. Grepl, N. C. Nguyen, K. Veroy, A. T. Patera, and G. R. Liu. Certified rapid solution of parametrized partial differential equations for real-time applications. In *Proceedings of the 2nd Sandia Workshop of PDE-Constrained Optimization: Towards Real-Time and On-Line PDE-Constrained Optimization*, SIAM Computational Science and Engineering Book Series, 2006. To Appear.
- [13] M. A. Grepl and A. T. Patera. Reduced-basis approximation for time-dependent parametrized partial differential equations. *M2AN Math. Model. Numer. Anal.*, 39:157–181, 2005.
- [14] G.F. Hawkins, E.C. Johnson, and J.P. Nokes. Detecting manufacturing flaws in composite retrofits. *SPIE*, 3587:97–104, 1999.
- [15] K. Ito and S. S. Ravindran. A reduced-order method for simulation and control of fluid flows. *Journal of Computational Physics*, 143(2):403–425, July 1998.
- [16] J. P. Kaipio, V. Kolehmainen, E. Somersalo, and M. Vauhkonen. Statistical inversion and monte carlo sampling methods in electrical impedance tomography. *Inverse Problems*, 16:1487–1522, 2000.
- [17] L. Machiels, Y. Maday, I. B. Oliveira, A. T. Patera, and D.V. Rovas. Output bounds for reduced-basis approximations of symmetric positive definite eigenvalue problems. *C. R. Acad. Sci. Paris, Série I*, 331(2):153–158, July 2000.
- [18] Y. Maday, A. T. Patera, and D. V. Rovas. A blackbox reduced-basis output bound method for noncoercive linear problems. In D. Cioranescu and J.-L. Lions, editors, *Nonlinear Partial Differential Equations and Their Applications, Collège de France Seminar Volume XIV*, pages 533–569. Elsevier Science B.V., 2002.
- [19] D.W. Marquardt. An algorithm for least-squares estimation of nonlinear parameters. *SIAM*, 11(2):431–441, 1963.
- [20] K. Mosegaard and M. Sambridge. Monte carlo analysis of inverse problems. *Inverse Problems*, 18:R29–R54, 2002.
- [21] K. Mosegaard and A. Tarantola. Probabilistic approach to inverse problems. *International*

- Handbook of Earthquake and Engineering Seismology, Part A*, pages 237–265, 2002.
- [22] N. C. Nguyen. *Reduced-Basis Approximations and A Posteriori Error Bounds for Nonaffine and Nonlinear Partial Differential Equations: Application to Inverse Analysis*. PhD thesis, Singapore-MIT Alliance, National University of Singapore, Singapore, 2005.
- [23] N. C. Nguyen, K. Veroy, and A. T. Patera. Certified real-time solution of parametrized partial differential equations. In S. Yip, editor, *Handbook of Materials Modeling*, pages 1523–1559. Springer, 2005.
- [24] I. B. Oliveira and A. T. Patera. Reduced-basis techniques for rapid reliable optimization of systems described by parametric partial differential equations. *Optimization and Engineering*, 2006. To appear.
- [25] T. A. Porsching. Estimation of the error in the reduced basis method solution of nonlinear equations. *Mathematics of Computation*, 45(172):487–496, October 1985.
- [26] C. Prud’homme, D. Rovas, K. Veroy, Y. Maday, A.T. Patera, and G. Turinici. Reliable real-time solution of parametrized partial differential equations: Reduced-basis output bounds methods. *Journal of Fluids Engineering*, 124(1):70–80, Mar 2002.
- [27] A. Quarteroni and A. Valli. *Numerical Approximation of Partial Differential Equations*. Springer, 2nd edition, 1997.
- [28] M.A. Starnes. *Development of Technical Bases for Using Infrared Thermography for Nondestructive Evaluation of Fiber Reinforced Polymer Composites Bonded to Concrete*. PhD thesis, Massachusetts Institute of Technology, September 2002.
- [29] A. N. Tikhnov. Solution of incorrectly formulated problems and the regularization method. *Soviet Mathematics Doklady*, 4(4):1035–1038, 1963.
- [30] A. N. Tikhnov and V. Arsenin. *Solution of Ill-Posed Problems*. John Wiley and Sons, 1977.
- [31] A.N. Tikhonov, A.V. Goncharsky, V.V. Stepanov, and A.G. Yagola. *Numerical Methods for the Solution of Ill-Posed Problems*. Kluwer Academic, Dordrecht, 1995.
- [32] Kim-Chuan Toh. Primal-dual path-following algorithms for determinant maximization problems with linear matrix inequalities. *Comput. Optim. Appl.*, 14(3):309–330, 1999.
- [33] K. Veroy. *Reduced-Basis Methods Applied to Problems in Elasticity: Analysis and Applications*. PhD thesis, Massachusetts Institute of Technology, Cambridge, MA, June 2003.
- [34] K. Veroy and A. T. Patera. Certified real-time solution of the parametrized steady incompressible navier-stokes equations; rigorous reduced-basis *a posteriori* error bounds. *International Journal for Numerical Methods in Fluids*, 47:773–788, 2004.
- [35] K. Veroy, D. Rovas, and A. T. Patera. *A Posteriori* error estimation for reduced-basis approximation of parametrized elliptic coercive partial differential equations: “Convex inverse” bound conditioners. *Control, Optimisation and Calculus of Variations*, 8:1007–1028, June 2002. Special Volume: A tribute to J.-L. Lions.
- [36] A.T. Watson, J.G. Wade, and R.E. Ewing. Parameter and system identification for fluid flow in underground reservoirs. In H.W. Engl and J. McLaughlin, editors, *Inverse Problems and Optimal Design in Industry*. Teubner, Stuttgart, 1994.